COMPUTATIONAL ANALYSIS OF HEAT TRANSFER ENHANCEMENT IN TUBES USING CAPSULE DIMPLED SURFACES AND AL_2O_3-WATER NANOFLUID

MAHMOUD AWNI A. HAJ IBARHIM

SEPTEMBER 2021

ÇANKAYA UNIVERSITY

GRADUATE SCHOOL OF NATURAL AND APPLIED SCIENCES

DEPARTMENT OF MECHANICAL ENGINEERING
MASTER DEGREE IN MECHANICAL ENGINEERING

COMPUTATIONAL ANALYSIS OF HEAT TRANSFER ENHANCEMENT IN TUBES USING CAPSULE DIMPLED SURFACES AND AL_2O_3-WATER NANOFLUID

MAHMOUD AWNI A. HAJ IBRAHIM

SEPTEMBER 2021

Approval of the Thesis**: Computational Analysis of Heat Transfer Enhancement in Tubes Using Capsule Dimpled Surfaces and Al_2O_3-Water Nanofluid**

Submitted by **MAHMOUD AWNI A. HAJ IBRAHIM**

Approval of the Graduate School of Natural and Applied Sciences, Çankaya University

_____

Assoc. Prof. Dr. Ziya ESEN

Director

I certify that this thesis satisfies all the requirements as a thesis for the degree of Master of Science.

_____

Prof. Dr. Haşmet TÜRKOĞLU

Head of Department

This is to certify that we have read this thesis and that in our opinion it is fully adequate, in scope and quality, as a thesis for the degree of Master of Science.

_____	_____
Asst. Prof. Dr. Ekin ÖZGİRGİN YAPICI	Prof. Dr. Haşmet TÜRKOĞLU
Supervisor	Co-Supervisor

Examination Date: 13.09.2021

Examining Committee Members:

Prof. Dr. Haşmet TÜRKOĞLU	Çankaya Univ.	_____
Assoc. Prof. Munir ELFARRA	Ankara Yıldırım Beyazıt Univ.	_____
Asst. Prof. Dr. Nureddin DİNLER	Gazi Univ.	_____
Asst. Prof. Dr. Ekin ÖZGİRGİN YAPICI	Çankaya Univ.	_____
Asst. Prof. Dr. Ülkü Ece AYLI İNCE	Çankaya Univ.	_____

STATEMENT OF NON-PLAGIARISM

I confirm that all information provided in this thesis is taken and presented according to the academic and ethical conduct which requires the referencing and citation of any material that are not original of this thesis.

Name, Last Name	: Mahmoud Awni A. Haj Ibrahim
Signature	:
Date	: 13.09.2021

ABSTRACT

COMPUTATIONAL ANALYSIS OF HEAT TRANSFER ENHANCEMENT IN TUBES USING CAPSULE DIMPLED SURFACES AND AL_2O_3-WATER NANOFLUID

Mahmoud Awni A. HAJ IBRAHIM

M.Sc., Department of Mechanical Engineering

Supervisor: Assist. Prof. Dr. Ekin ÖZGIRGIN YAPICI

Co-Supervisor: Prof. Dr. Haşmet TÜRKOĞLU

SEPTEMBER 2021, 70 Pages

This study aims to numerically investigate the enhancement of heat transfer by utilizing geometrical configurations as capsule dimples on tube surfaces. Two working fluids, water and Al_2O_3-water nanofluid, are used under uniform heat flux applied to the tube surface. The originality of this work lies in combining two passive heat transfer enhancement methods, using geometrical improvements and nanofluids together. Capsule dimples are used at different depths, such as 1 mm, 1.5 mm, 2 mm and 2.5 mm for each case. Al_2O_3-water nanofluid modeled as a single-phase fluid at three different nanoparticle concentrations of 1%, 2% and 3%. The effects of dimple depth and nanofluids in different nanoparticle concentrations on Nusselt number, friction factor and performance evaluation criteria (PEC) which are widely used in heat transfer enhancement evaluation, were studied. Numerical studies were performed using ANSYS 20R1 Fluent commercial software in the 2000-14000 Reynolds number range and inlet fluid temperature of 293°K. The turbulence is modelled using the realizable k-ε model.

It was found that for laminar, transient and fully developed turbulent flows, as the dimple depth increases, the Nusselt number as well as the friction factor increases for both cases of water and Al_2O_3-Water nanofluid as working fluids. The Nusselt number for dimpled tubes is enhanced by 41.3% and 46.3% compared to plain tubes for water and nanofluid with 3% concentration, respectively. Furthermore, the variation of PEC for capsule dimpled tubes are dependent on flow regions and dimple depths. Generally, increasing the nanofluid volume concentration and dimple depth in laminar flows increases PEC significantly. Among all simulated cases, for laminar flow PEC would vary up 5.5 when dimple depth is 2.5 mm and volume concentration is 3%. In transition flows, PEC = 1.2 for 2 mm depth and 3% volume concentration. Lastly, for fully turbulent flows considered the highest PEC is obtained as 1.057 in the case of 1 mm depth and 1% volume concentration.

Keywords: Heat transfer enhancement, Nanofluid, Dimpled tubes, Computational analysis, Performance evaluation criteria (PEC).

ÖZ

BORU YÜZEYİNDEKİ KAPSÜL TİPİ KABARTMANIN VE AL_2O_3-SU NANO AKIŞKANIN ISI TRANSFERİNE ETKİSİNİN SAYISAL ANALİZİ

Mahmoud Awni A. HAJ IBRAHIM

Yüksek Lisans, Makine Mühendisliği Anabilim Dalı

Tez Yöneticisi: Dr. Öğr. Üyesi. Ekin Özgirgin Yapıcı

Eş-Yönetici: Prof. Dr. Haşmet TÜRKOĞLU

EYLÜL 2021, 70 Sayfa

Bu çalışmada, duvar yüzeyinden üniform ısı akısı uygulanan boru içi akışlarda boru yüzeyine yapılan geometrik modifikasyonların ısı transferi iyileştirmeye etkileri sayısal olarak incelenmiştir. Geometrik modifikasyon olarak kapsül tipi kabartmalar kullanılmış, akışkan olarak ise su ve Al_2O_3-su nano-akışkan kullanılmıştır. Isı transferi iyileştirmesi için hem geometrik modifikasyon yapılmış olması hem de bununla birlikte farklı nano partikül yüzdelerinde nano-akışkan kullanılmış olması çalışmayı benzerlerinden farklılaştırmaktadır.

Kapsül tipi kabartmalar borunun iç yüzeyine farklı derinliklerde (1 mm, 1.5 mm, 2 mm ve 2.5 mm) uygulanmıştır. Al_2O_3-su nano-akışkan hacimsel konsantrasyon oranları %1, %2 ve %3 olarak ele alınmıştır. Akış tek fazlı akış olarak modellenmiş ve uygulanmıştır. Kabartmaların derinliğinin ve nono-akışkanın farklı konsantrasyonlarda uygulamalarının Nusselt sayısı, sürtünme katsayısı ve performans değerlendirme kriteri (PEC) üzerindeki etkileri analiz edilmiştir. Sayısal analizler ANSYS 20R1 Fluent kullanılarak 2000-14000 Reynolds sayısı aralığında reliazable k-ε türbülans modeli ile yapılmıştır.

Sonuçlar incelendiğinde, tüm akışkanlar için, laminer akış, geçiş akışı ve tamamen gelişmiş türbülanslı akış durumunda kabartma derinliği arttıkça Nusselt Sayısı ve aynı zamanda da sürtünme katsayısının arttığı görülmüştür. Düz boruda su akışı ile kıyasladığında, akışkan su olduğunda kabartmalı boruda ısı transferi %41.3, kabartma artı %3 konsantrasyonlu nano-akışkan kullanılan boruda ise ısı transferi %46.3 iyileştirilmiştir. Performans değerlendirme kriterinin değişimi akış rejimine ve kabartma derinliğine oldukça bağlıdır. Genel olarak, laminer akışta nano-akışkan konsantrasyonu ve kabartma derinliği arttıkça performans değerlendirme kriterinin önemli ölçüde arttığı görülmüştür.

Çalışılmış tüm simülasyon sonuçları incelendiğinde; laminer akışta en yüksek PEC 5.5 olarak %3 nano-akışkan konsantrasyonu ve 2.5 mm kabartma kalınlığında gözlemlenmiştir. Geçiş akışında en yüksek PEC 1.2 olarak %3 nano-akışkan konsantrasyonu ve 2 mm kabartma kalınlığında, türbülanslı akışta ise en yüksek PEC 1.057 olarak %1 nano-akışkan konsantrasyonu ve 1 mm kabartma kalınlığında gözlemlenmiştir.

Anahtar Kelimeler: Isı transferi iyileştirmesi, Nano-akışkan, Kabartmalı boru, Hesaplamalı Akışkan Dinamiği, Performans değerlendirme kriteri

ACKNOWLEDGMENTS

First of all, thanks to Allah for giving me knowledge, strength and patience.

Secondly, I would like to express my deepest appreciation to my supervisor Dr. Ekin ÖZGİRGİN YAPICI for her patient guidance, enthusiastic encouragement and useful critiques of this research work. I would also like to extend my deepest gratitude to my co-supervisor Prof. Dr. Haşmet TÜRKOĞLU for his invaluable and constructive suggestions to improve the quality of this research, for which I am thankful and honored.

I would like to express my special appreciation and gratefulness to my parents for their constant prayers and love, without them I would not be the person I am today. Also, my gratitude goes to my brothers and sisters for their ultimate support and encouragement.

I gratefully acknowledge the assistance of my friend Osama NSAIF for many of the stages throughout my work on this thesis.

Finally, I would like thank all my friends and everyone who had a direct or indirect contribution to this accomplishment.

TABLE OF CONTENTS

LIST OF FIGURES

LIST OF TABLES

SYMBOLS

Δp	pressure difference (Pa)
c_p	specific heat, (J.kg^{-1}.K)
D_h	hydraulic diameter, (m)
f	friction factor
h	heat transfer coefficient, (W.m^{-2}.K)
k	thermal conductivity, (W.m^{-1}.K)
L	tube length, (m)
Nu	average Nusselt number
$\dot{m}$	mass flow rate, (kg/s)
P	pressure, (Pa)
Pr	Prandtl number
PEC	performance evaluation criteria
$\dot{q}$	heat flux, (W/m^2)
Re	Reynolds number
T	temperature, (K)
U	mean velocity, (m/s)
u_*	friction velocity
y^+	near wall mesh resolution

SUBSCRIPTS

bf	base fluid
d	dimple
h	hydrodynamic
in	inlet
nf	nanofluid
m	mean
out	outlet
p	plain
s	surface
t	thermal
w	wall
x	location on x-direction

GREEK LETTERS

φ	volume concentration of nanoparticle
ρ	density, (kg/m^3)
μ	viscosity (Pa.s)
τ	wall shear stress, (Pa)

CHAPTER 1

INTRODUCTION AND LITERATURE REVIEW

1.1. MOTIVATION AND AIM OF THE STUDY

Tube heating or cooling is a field of interest for many researchers and academicians due to its usability and accessibility in many engineering and industrial applications. Such applications include heat exchangers, which are widely used in refrigeration, air conditioning, space heating, power generation and chemical processing for cooling or heating purposes, district heating systems, renewable energy systems, geothermal water distribution systems, particularly solar collectors, geothermal water distribution systems, and so on.

In the variety of these applications, the main challenge is to increase the heat transfer performance of the systems per unit area or volume. Of concern in this topic is that for a variety of applications, an increase in heat transfer performance becomes necessary but the limits of sizing prevent the achievement of this goal. This challenge offers an opportunity for improvement to develop methods to make heat transfer equipment compact and to achieve a high heat transfer rate using minimum pumping power to minimize the cost of energy and materials. The most effective method of heating or cooling is to increase the heat transfer coefficients on the hot and cold fluid sides and this can be accomplished by one or more active or passive methods.

Methods that provide improvements in heat transfer by giving additional energy are called active methods, which include surface vibration and flow vibration, electrostatic fields and mechanical aids. Methods that improve heat transfer without additional energy are called the passive method. These include applying geometrical modifications to increase the heat transfer surface area or using additives in the working fluid, such as nanoparticles. Passive methods are more advantageous than active methods such that they do not require external energy and are easier to apply and provide enhancement easily. These methods are explained in the next part.

There is great demand to find better and alternative solutions to elevate heat transfer performance for different applications in heated or cooled tubes. From this standing point, the aim of this study is to examine and apply methods to enhance the thermal behavior and performance of heat transfer in heated tubes by using different fluids and geometrical improvements.

According to a review study regarding this topic, much research has been conducted. A remarkable method has been developed to enhance heat transfer for tubular systems by placing turbulators in the flow domain inside the tube or by using nanofluids as a working fluid instead of water or ethanol-glycol.

In this study, methods for heat transfer enhancement were sought and the most effective methods that were chosen included dimples and nanofluids. The simulated problem was carried out on a capsule dimpled tube (Figure 1.1) with water and Al_2O_3-water nanofluid as heat transfer fluids and constant heat flux applied uniformly on a tube surface. The effect of different dimple depths and different nanoparticle concentrations on heat transfer enhancement were studied and analyzed. ANSYS 20R1 was used for mesh generation and simulations in all cases.

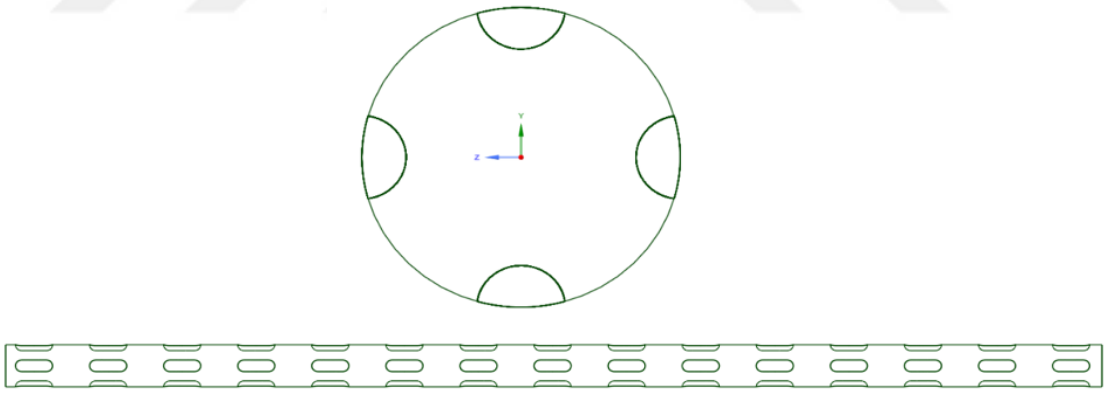

Figure 1.1 Schematic of capsule dimpled tube.

1.2. METHODS FOR HEAT TRANSFER ENHANCEMENT.

In recent years, scientists have focused on developing passive techniques to improve heat transfer characteristics in heat exchangers. To enhance the efficiency of the heat transfer of these methods, numerical and experimental investigations have

been performed. As a result of the need to decrease the costs and sizes of heat exchangers, scientists have been examining alternative methods of heat transfer improvement. Due to their simplicity and applicability in a wide range of applications, passive heat transfer improvement methods are type that are the mostly used. These include rough surfaces, expanded surfaces such as wire coiled tubes, bent band pieces, screw type rotating pieces, twisted tapes, winding wires, guiding wings and flow rotating propellers. Dimples are examples of passive methods and they include additional additives to the working fluid. Passive methods also do not require any external power input other than to transport the fluid. Refrigerators, ventilation, heat pumps and many more industries rely on tubes with varied inserts that are improved with different materials. Inserts in tubular heat exchangers not only reduce heat exchanger dimensions but also produce thermal, mechanical and economic improvements in heat exchangers.

1.2.1. Geometrical Improvement

1.2.1.1. Louvered Strip Insert

To increase heat transfer, louvered strip inserts can be used by changing inclination angles, distances between wings, the forms of the wings as well as the direction of flow. Figure 1.2 shows forward and backward louvered strips. Using louvered strips, Eiamsa-Ard et al. (2008) found that the overall backward flow performed better than the forward flow.

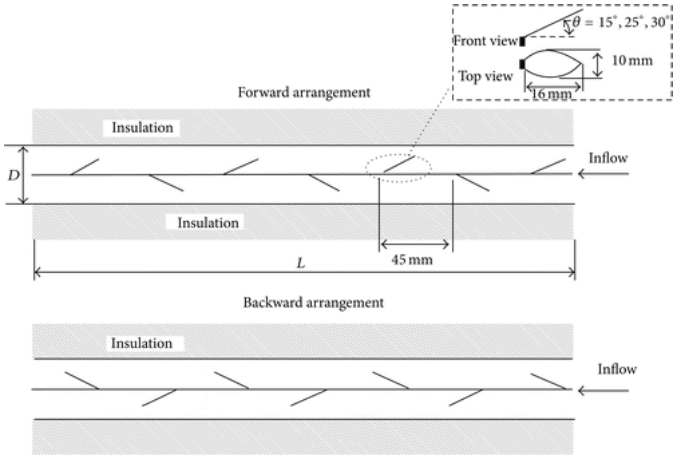

Figure 1.2 Forward and backward arrangements of louvered strips (Eiamsa-Ard et al., 2008).

1.2.1.2. Twisted Tapes

To enhance heat exchange rates and abilities, heat exchanger tubing is supplied with twisted tapes (twisted turbulators) to increase the turbulent flow characteristics through the tube. This device mixes the fluid or gas inside the tube and increases the heat transfer coefficient (Tabatabaeikia et al., 2014).

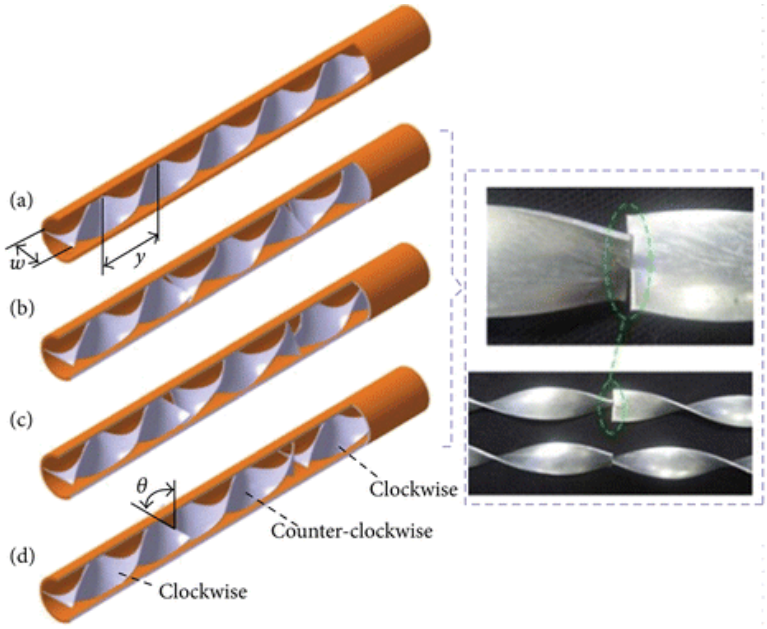

Figure 1.3 Design of alternate clockwise and counter-clockwise twisted tapes.

1.2.1.3. Helical Screw Insert

Figure 3.3 shows a circular tube equipped with helical twist inserts. Thermal performance investigation had been made on such helical twist inserts (Pathipakka et al., 2010). The outcomes show that an increase in the Reynolds number has a greater effect on the improvement of heat transfer, whereas increasing the twist ratio will reduce the heat transfer improvement.

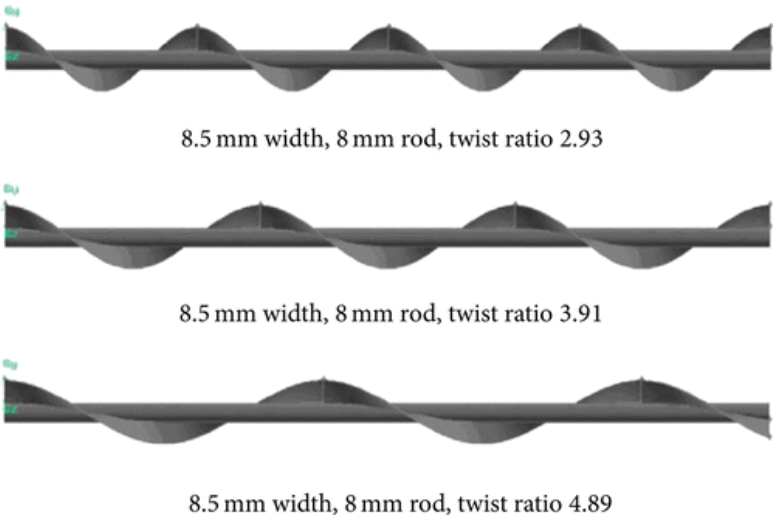

Figure 1.4 Schematic diagram of helical tape inserts.

1.2.1.4. Wire Coil Insert

According to research on the influence of coil-wire inserts on heat transfer properties, tubes with coil-wire inserts (Figure 1.4) had a greater heat transfer coefficient than the plain tube. Investigations into heat transfer enhancement during forced convection-condensation of R-22 revealed that the tube with the thickest wire may reach its maximum heat transfer enhancement (Chandrasekar et al., 2013).

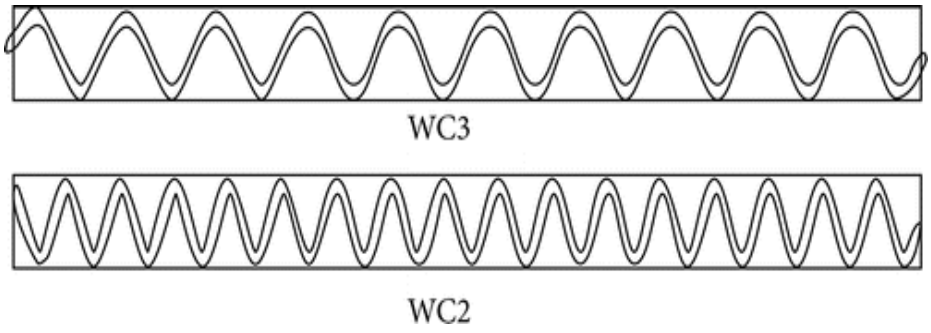

Figure 1.5 Wire coil inserts.

1.2.1.5. Internal Fined Tube

Fines inside tubes have been used as a heat transfer enhancement method recently. Mohapatra and Mishra (2015) conducted a numerical study on a tube with internal wall fins, as presented in Figure 1.5. Four fin shapes where studied, triangular, rectangular, trapezoidal and the T-shape, as seen in Figure 1.6, to observe the best hydrodynamic and thermal characteristics. The T-shaped fin proved to have the highest

thermal performance and highest pressure drop due to the ability of this shape to provide better turbulent generation.

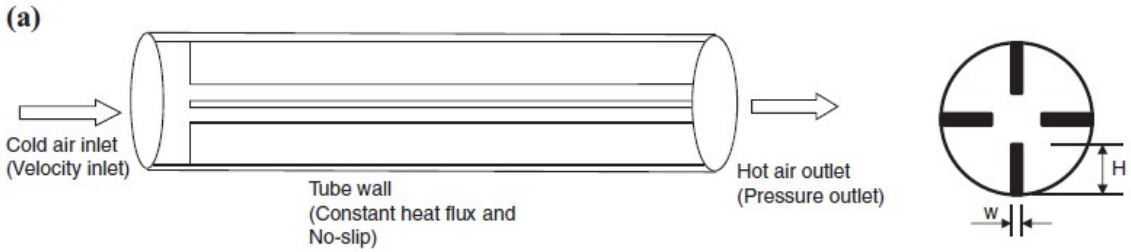

Figure 1.6 Schematic of internal wall fins.

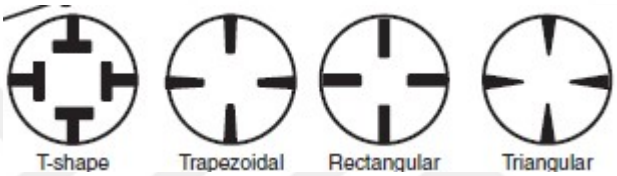

Figure 1.7 Different types of internal wall fins.

1.2.1.6. Dimpled Geometries

Another common passive method used in modifying heat transfer is through the application of dimples on the tube surface. A reason for this is to increase the area in which heat transfer occurs. The considerable effects obtained by Li et al. (2015), both experimentally and numerically on a dimpled tube (Figure 1.7) showed an enhancement in overall thermal performance compared to normal tubes. Details of this topic is given in Section 1.3.

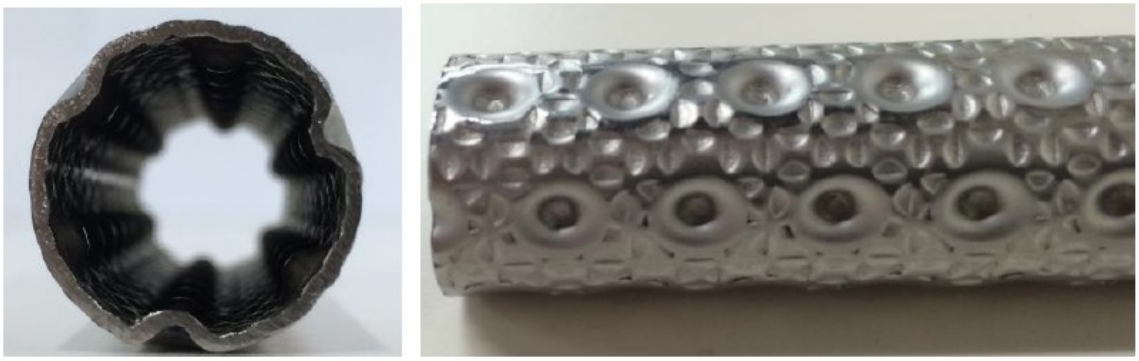

Figure 1.8 Modified tube surface using dimples.

1.2.2. Improvement with Nanofluids

The use of nanofluids in many research applications has been of interest to researchers, most especially in the heat transfer and fluid dynamics communities due to it their incredible advantages in improving performance wherever they are used. The upcoming discussion will highlight on some of the applications that showed enhancement through the adoption of nanofluids.

1.2.2.1. Applications for Car Radiators

In this experimental study conducted by Peyghambarzadeh et al. (2011) on a coolant car radiator, as seen in Figure 1.7, different nanofluids such as Al_2O_3-water and Al_2O_3-ehylene glycol as coolants, are compared in terms of practical enhancement in heat transfer. It was found that the adoption of nanofluids has an economical benefit, such as reducing the size of heat exchangers used for cooling car engines.

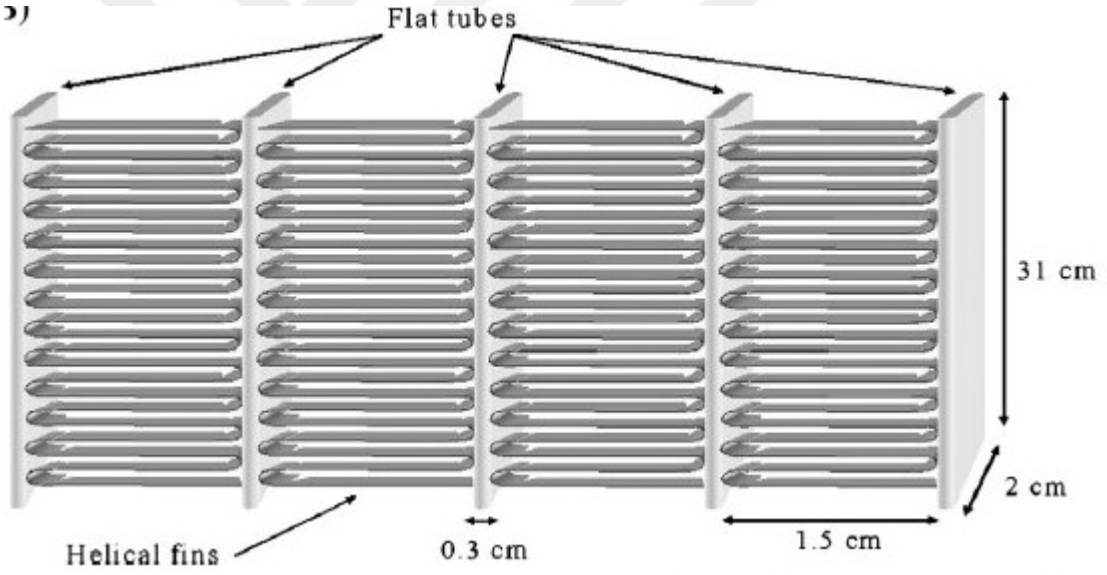

Figure 1.9 Cross-section of a heat exchanger in a car radiator.

1.2.2.2. Applications for Electronic Components

In computers, one of the most important parts in which to maintain a stabilized cooling temperature is the graphic processing unit (GPU), which is essential for handling heavy duty working software and games, as shown in Figure 1.8. An experimental investigation using an Ag-Water nanofluid on cooling a GPU attached to a heat sink, as in Figure 1.9, was conducted by Siricharoenpanich et al. (2021), which showed a reduction in thermal resistance and indicated an increase in overall cooling performance.

Figure 1.10 GPU attached to a heat sink with nano fluid.

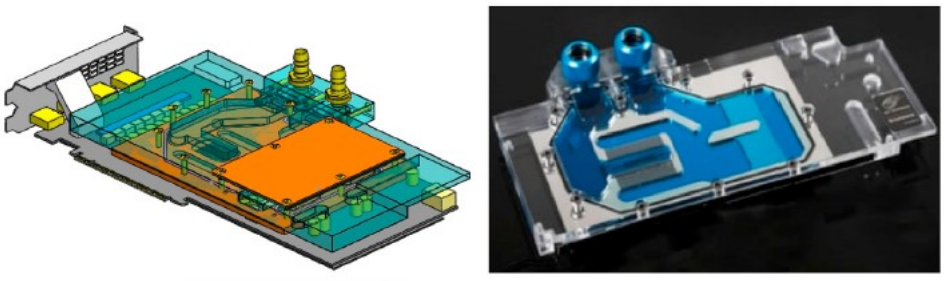

Figure 1.11 Heat sink used in the experiment.

1.2.2.3. Applications for Heat Pipes

Heat pipes are the largest applications in adopting and experimenting with nanofluids due to durability and accessibility in terms of observing the improvement in flow characteristics. As an example, Menlik et al. (2014) worked on a heat pipe using a MgO-Water nanofluid as a heat transfer fluid to investigate the improvements

caused by this fluid (see Figure 1.10). The results provided a clear enhancement in the working heat pipe efficiency indicating an increase in the heat transfer performance.

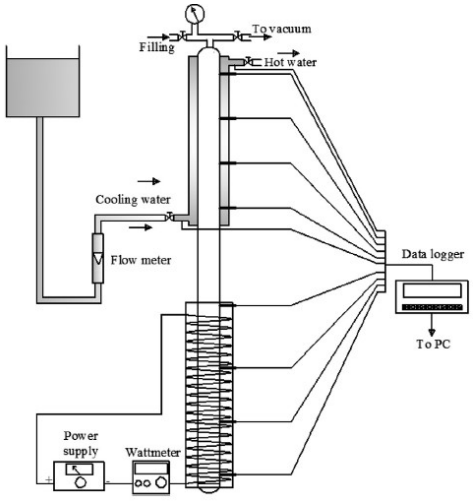

Figure 1.12 Experimental schematic of a heat pipe (Menlik et al., 2014).

1.3. LITERATURE REVIEW

1.3.1. Literature Review on Geometrical Enhancement

Cheraghi et al. (2020) conducted a numerical study on a new configuration of deep dimpled tubes under constant heat flux to evaluate the effect of different pitches, dimple diameters and dimple depths on the thermal fluid characteristics and flow field for Reynolds numbers 500, 1,000 and 2,000. The study showed that decreasing the distance between dimples while incrementing the dimple depth and diameter would result in increasing the Nusselt number and friction factor. The sudden growth in the friction factor is due to the creation of vortexes behind each dimple causing the pressure drop to be larger than in the plain tubes. According to the performance evaluation criteria, the highest performance enhancement for the deep dimpled tube can be achieved by increasing the dimple diameter, pitch and Reynolds number and reducing the dimple depth.

Wang et al. (2010) carried out an experimental study on a heat exchanger with ellipsoidal and spherical dimpled tubes. The working fluids used in their experiments were hot water on the shell side and cold air on the dimpled tube. Comparisons were made for ellipsoidal, spherical and smooth tubes in terms of the effects observed on the previously mentioned tubes on hydrodynamics and heat transfer. Both ellipsoidal and spherical dimpled tubes showed an enhancement compared to the smooth tube,

whereas the ellipsoidal dimples proved to have the best performance among them all for Reynolds numbers ranging between 1,500 and 60,000.

Kumar et al. (2017) experimentally and numerically investigated different span-wise and stream-wise directions on the heat transfer and hydrodynamics performance of dimpled tubes having Reynolds numbers between 4,000 and 28,000 and air as a working fluid. The study showed that the highest Reynolds numbers cause the highest Nu and lowest friction factor as expected. On the other hand, increasing the stream and span-wise direction to a certain extent would have a positive effect on heat transfer enhancement, and thermal hydraulics performance would increase if the stream and span-wise directions decrease. The author revealed that the optimum performance for thermal and hydraulic performance are reached when stream and span-wise direction had the value of 15.

Vicente et al. (2002) conducted a detailed experimental study on helically dimpled tubes covering a wide range of Reynolds numbers and Prandtl numbers to investigate the effect of two introduced non-dimensional parameters of Reduced Height and Dimple Density on the overall heat transfer and hydrodynamic performance. As a result, they showed that reduced height has the greatest influence in both the Nusselt number and friction factor, hence here being an increase in both heat transfer and pressure drop. On the other hand, dimple density showed no significant influence.

Chen et al. (2001) experimentally studied six different dimpled tubes at different dimple parameters, ratio of depth to tube diameter, depth to pitch ratio and number of dimples on the tube surface. The Reynolds numbers taken in this experiment had ranged from 7,500 to 52,000. It was found that the enhancement in heat transfer reached 137% compared to standard smooth tubes and the performance criteria showed values from 0.93 to 1.16 in which the dimpled tube with values above unity were considered to succeed in the performance enhancement.

Ming et al. (2016) undertook an experimental and numerical study to investigate the effect of dimpled tubes within a concentric tube heat exchanger on heat transfer and pressure drops with Reynolds numbers ranging from 500 to 8,000 for water as a working fluid. An enhancement in the pressure drop ratio was observed on Reynolds numbers between 500 and 2,000 with the pressure drop becoming constant above Re = 2,000. On the other hand, heat transfer showed a greater enhancement

compared to a pressure drop, which results in an increase in the performance evaluation criteria (PEC).

Sabir et al. (2020) determined numerically the thermal and hydraulic performance of various dimples having spherical, conical and ellipsoidal shapes in addition to different ellipsoidal angler orientations in perpendicular and parallel patterns. As a result, ellipsoidal dimples showed an increase in the heat transfer rate in comparison to the conical and spherical shapes, whereas the effect of the angler orientation of the ellipsoidal dimples proved to enhance the heat transfer with pressure dropping significantly. Overall, 45 with parallel patterns showed the optimum performance according to the performance evaluation criteria.

1.3.2. Literature Review on Nanofluids (or Nanoparticles)

Khedkar et al. (2014) experimentally investigated the effect of different nanoparticle concentrations of a TiO_2-water base nanofluid on the heat transfer performance in a concentric tube heat exchanger; hence the use of nanofluid was for cooling purposes in which the inner tube was for the nanofluid and the outer tube was for water as a hot fluid. The coolant working range of this experiment had Reynolds numbers ranging from 300 to 4,000. For the sake of comparison, the authors repeated the experiments for water as a coolant to evaluate the difference in performance. They investigated the effects of different nanoparticle concentrations (2% and 3%) of nanofluid and showed that increasing the Reynolds number proved to result in a significant increase in heat transfer performance compared to water as a cooling fluid.

Ho et al. (2018) preformed experimental investigations on a tube with circular cross sections under constant heat flux for laminar flow with Reynolds numbers ranging from 120 to 2,000 using an Al_2O_3-water nanofluid as a working fluid. To evaluate the effects of the nanofluid subjected to variable operating temperatures on heat transfer characteristic and pressure differences, an additional numerical study was conducted. The results proved that using Al_2O_3 nanoparticles in water based nanofluid for forced heat transfer applications would minimize the temperature difference between the fluid mean temperature and wall temperature that results in a better heat transfer characteristic but with an increasing pressure drop.

Briclot et al. (2020) undertook an experimental study in heated tubes with an Al_2O_3-Water nanofluid for different nanoparticle volume concentrations in laminar and transition flow regions with Reynolds numbers ranging from 500 to 4,500. The

study showed that for the specified Reynolds numbers, the nanoparticle volume concentrations did not have any significant enhancement in the heat transfer coefficient. However, in terms of pressure drops, it showed an incremental increase in volume concentration.

Mehrjou et al. (2015) conducted an experiment on square ducts with a CuO-Water nanofluid as the working fluid for turbulent flow. Throughout their investigation, the enhancement in the Nusselt number and heat transfer coefficient showed a great dependency on the increase of the volume concentration of nanoparticles.

CHAPTER 2

MATHEMATICAL FORMULATION

2.1. INTRODUCTION

This chapter revolves around and discuss the governing equations necessary for mathematical modeling of flow heat transfer in a heated tube with and without capsule dimples. Water and nanofluids (water + nanoparticles) are considered to be the working fluid.

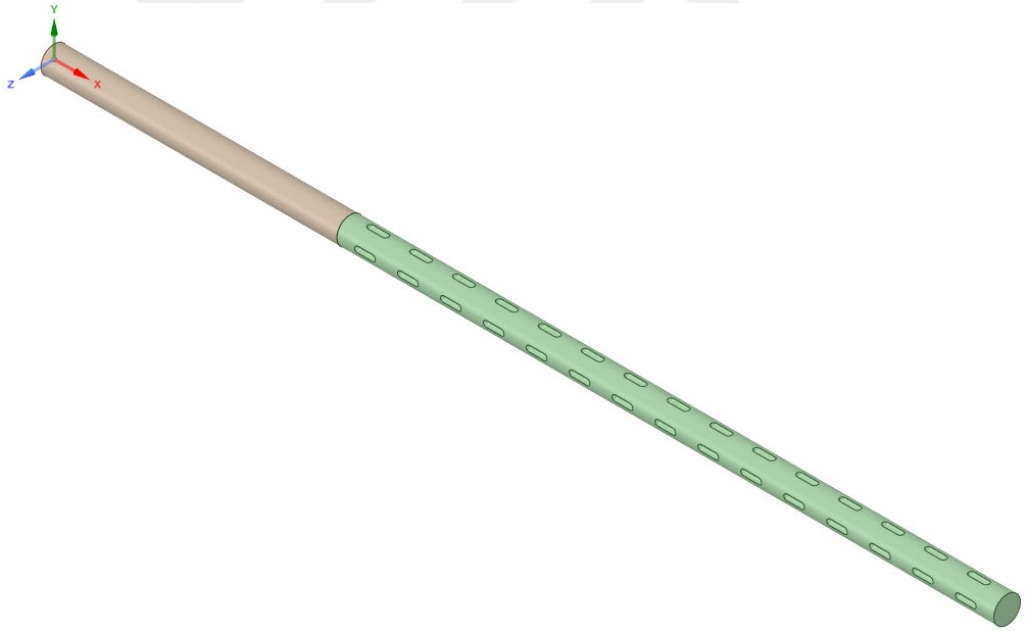

Figure 2.1 Capsule dimpled tube with entrance length.

2.2. NANOFLUID MODELLING

Generally, when dealing with nanofluids, there are two known methods for formulating and modeling their flow. Before diving into details, it is worth noting that nanofluids are composed of nano-scaled metallic particles, such as Al_2O_3 and TiO_2 dispersed into a base fluid such as water, ethylene glycol or oil.

2.2.1. Single-Phase Model for Nanofluids

This model is well known and commonly used when studying nanofluid flows, hence the single-phase model being used for the current study. The advantage of this model is that since the nanoparticles dispersed in the base fluid are at a nanoscale, it is easy to assume that these nanoparticles are in homogeneity with the base fluid. In other words, they share the same velocity and are in thermal equilibrium. The thermal properties of the nanofluid are then calculated using the equations proposed by different researchers in the literature. In the current study, the single-phase model is used.

2.2.2. Multi-Phase Model

In real practice, nanoparticles and base fluids can hardly be in homogeneity and nanoparticles and base fluids in a flow field may have different velocities and hardly reach thermal equilibrium. Euleriane-Mixture and Euleriane-Eulerian are well known multi-phase models (Göktepe et al., 2014) used to compute nanofluid flows. In these models starting with a Euleriane-Mixture, the governing equations of fluid dynamics are solved by correlating the velocity term for nanoparticles and base fluid followed by averaging them under one term, whereas for the Euleriane-Eulerian model, the governing equations are solved separately for nanoparticles and the base fluid.

2.2.3. Thermophysical properties of Nanofluids

The chosen flow model for dissolving nanoparticles-water mixture is assumed to be single flow, which represents the formulation and calculation of thermal properties to form a homogeneity between the nanoparticles and base fluid, which is presented in the following parts.

2.2.3.1. Density

Calculations of nanofluid density are carried out according to the Cho and Pak (1998) correlation valid for various volume concentrations.

$$\rho_{nf=(1-\varphi)\rho_{bf}+\varphi\rho_{np}} \tag{1}$$

where φ, bf and np refer to volume concentration, base fluid and nanoparticles, respectively.

2.2.3.2. Specific Heat

The effective specific heat of the nanofluid $(C_p)_{nf}$ can be calculated based on the Xuan and Roetzel (2000) relation:

$$(C_p)_{nf} = \frac{(1-\varphi)(\rho C_p)_{bf} + \varphi(\rho C_p)_{np}}{\rho_{nf}} \quad (2)$$

2.2.3.3. Thermal conductivity

The Maxwell's model (1954) for evaluating the thermal conductivity shown below

$$k_{nf} = \frac{k_{np}+2k_{bf}-2\varphi(k_{bf}-k_{np})}{k_{np}+2k_{bf}+\varphi(k_{bf}-k_{np})} k_{bf} \quad (3)$$

This model present the thermal conductivity of a nanofluid relying on k_{np}, k_f and φ, which respectively represent the thermal conductivity of spherical nanoparticles, thermal conductivity of the fluid and the volume concentration.

2.2.3.4. Viscosity

The effective viscosity can be determined by the Batchelor (1977) model as follows.

$$\mu_{nf} = \mu_{bf}(1 + 2.5\varphi) \quad (4)$$

For prediction the effective viscosity of Al_2O_3, Pak and Cho (1998) developed a model for this purpose (used in current study).

$$\mu_{nf} = \mu_{bf}(1 + 39.11\varphi_{np} + 533.9\varphi^2_{np}) \quad (5)$$

2.3 GOVERNING EQUATIONS FOR THE FLUID FLOW

To derive the governing equations for the current physical problem, conservation of mass, Newton's Second Law and the Law of Conservation of Energy are mathematically formulated. The assumptions for deriving these equations are considered to be:

- Three-dimensional flow
- Steady flow
- Viscous and incompressible flow
- Turbulent flow
- Effect of body force being neglected
- Working fluids having constant properties
- Newtonian fluids

In addition, it is assumed that the particle distribution (mass fraction) in the flow field is uniform, nanoparticles and the base fluid are in thermal equilibrium, and the velocities of the nanoparticles and base fluid are equal. The physical properties of the nanoparticle-water mixture are calculated using the correlations in the literature. Below are the governing equations:

2.3.1. Continuity Equations

The derivation of the continuity equation is based on the law of conservation of mass, which is derived considering the previously mentioned assumptions.

$$\frac{\partial \bar{u}}{\partial x} + \frac{\partial \bar{v}}{\partial y} + \frac{\partial \bar{w}}{\partial z} = 0 \tag{6}$$

knowing that $\bar{u}$, $\bar{v}$ and $\bar{w}$ are the time average velocity components in the x, y and z directions, respectively.

2.3.2. Navier-Stokes Equations (Momentum Equations)

The momentum equations are formulated out of the Newton's Second Law. In each coordinate direction, Reynold averaged the Navier-Stokes equations given as below for a turbulent flow:

x direction:

$$\rho_{nf}\left(\bar{u}\frac{\partial \bar{u}}{\partial x} + \bar{v}\frac{\partial \bar{u}}{\partial y} + \bar{w}\frac{\partial \bar{u}}{\partial z}\right) = -\frac{\partial p}{\partial x} + \mu_{nf}\left(\frac{\partial^2 \bar{u}}{\partial x^2} + \frac{\partial^2 \bar{u}}{\partial y^2} + \frac{\partial^2 \bar{u}}{\partial z^2}\right) - \left(\frac{\partial \overline{u'^2}}{\partial x} + \frac{\partial \overline{u'v'}}{\partial y} + \frac{\partial \overline{u'w'}}{\partial z}\right) \tag{7}$$

y direction:

$$\rho_{nf}\left(\bar{u}\frac{\partial \bar{v}}{\partial x} + \bar{v}\frac{\partial \bar{v}}{\partial y} + \bar{w}\frac{\partial \bar{v}}{\partial z}\right) = -\frac{\partial p}{\partial y} + \mu_{nf}\left(\frac{\partial^2 \bar{v}}{\partial x^2} + \frac{\partial^2 \bar{v}}{\partial y^2} + \frac{\partial^2 \bar{v}}{\partial z^2}\right) - \left(\frac{\partial \overline{v'u'}}{\partial x} + \frac{\partial \overline{v'^2}}{\partial y} + \frac{\partial \overline{v'w'}}{\partial z}\right) \tag{8}$$

z direction:

$$\rho_{nf}\left(\bar{u}\frac{\partial \bar{w}}{\partial x} + \bar{v}\frac{\partial \bar{w}}{\partial y} + \bar{w}\frac{\partial \bar{w}}{\partial z}\right) = -\frac{\partial p}{\partial z} + \mu_{nf}\left(\frac{\partial^2 \bar{w}}{\partial x^2} + \frac{\partial^2 \bar{w}}{\partial y^2} + \frac{\partial^2 \bar{w}}{\partial z^2}\right) - \left(\frac{\partial \overline{w'u'}}{\partial x} + \frac{\partial \overline{w'v'}}{\partial y} + \frac{\partial \overline{w'^2}}{\partial z}\right) \tag{9}$$

In these equations, $\bar{u}$, $\bar{v}$ and $\bar{w}$ are time averaged velocity components in the x, y and z directions, respectively, and p, ρ_{nf} and μ_{nf} denote the pressure, effective density (mixture density) and effective viscosity (mixture viscosity) of the nanofluid, respectively.

2.3.3. Energy Equation

From the First Law of Thermodynamics, the energy equation is derived:

$$div\ (\rho_{nf}\bar{V}C_{p,nf}\bar{T}) = div\left(k_{nf}\ grad\ (\bar{T}) - \rho_{nf}\overline{T'}C_{p,nf}\overline{V'}\right) \quad (10)$$

where, k_{nf} is the effective thermal conductivity and $C_{p,nf}$ is the effective specific heat of the nanofluid.

Boundary conditions concerning the present study are as follows:

- The velocity inlet being defined using a Reynolds number ranging from 2,000 to 14,000;
- A constant inlet temperature of 293°K;
- A uniform heat flux being applied along the tube surface (10,000 W/m^2); and
- A 0 Pa gauge pressure outlet.

Further explanations regarding boundary conditions are found in Chapter 3.

2.4. IMPORTANT PARAMETERS OF FLUID FLOW

2.4.1. Reynolds Number

The Reynolds number is the ratio of the force of inertia to the viscous force for any flow and it is one of the most important parameters used to characterize fluid flows. The Reynolds number is defined thus:

$$\mathrm{Re} = \frac{\rho_{nf}\mathrm{UD_h}}{\mu_{nf}} \quad (11)$$

where ρ is the fluid density, U the average velocity, D_h the hydrodynamic diameter (for circular tube D_h being the same as the tube diameter) and μ is the dynamic viscosity. If the Reynolds number is lower than a certain value, which is approximately 2,000 for internal flow, flow is said to be laminar, and if it exceeds this value, flow becomes turbulent.

2.4.2. The Nusselt Number

The Nusselt number is considered to be a standard way to express the heat transfer rate between fluid and solid surfaces, which has the physical meaning of the convection heat transfer relative to conduction heat transfer within a fluid layer (Cengel, 2014)

$$\mathrm{Nu} = \frac{hD_h}{k_{nf}} \quad (12)$$

where h, k and D_h are the heat transfer coefficient, thermal conductivity and hydraulic diameter of the tube, respectively.

The local Nu can be calculated using the following equations:

$$\mathrm{Nu}_x = \frac{h_x D_h}{k} \tag{13}$$

where

$$h_x = \frac{\dot{q}_s}{T_w - T_m(x)} \tag{14}$$

where $\dot{q}_s$ is the heat flux applied on the outer surface, $T_m(x)$ the mean (bulk) temperature of the fluid and T_w the wall temperature.

$$T_m(x) = T_{m,in} + \frac{\dot{q}_s \pi D_h}{\dot{m} C_p} x \tag{15}$$

where $T_{m,i}$, $\dot{m}$, C_p and x are respectively the mean temperature at the inlet, mass flow rate and specific heat of the fluid, and the distance from the dimpled tube inlet.

The average Nu can then be calculated as:

$$\overline{Nu} = \frac{1}{L}\int_0^L Nu(x)dx \tag{16}$$

2.4.3. Friction Factor

The friction factors for the plain tube and capsule dimpled tube are calculated using the Darcy friction factor for turbulent flows in a pipe (Cengel, 2014):

$$f = \frac{2D_h \Delta p}{\rho_{nf} L U^2} \tag{17}$$

The friction factor can also be derived by substituting the wall shear stress τ, in the Darcy friction factor:

$$f = \frac{8\tau}{\rho_{nf} \mathrm{U}^2} \tag{18}$$

The near wall mesh resolution is defined by:

$$\mathrm{y}^+ = \mathrm{y}\left(\frac{\mathrm{u}_*}{\mu}\right) \tag{19}$$

Note that y is the distance between the wall and the center of the cell adjacent to the wall.

And friction velocity u_* formulated as (Liu, 1974):

$$\mathrm{u}_* = \left(\frac{\mathrm{f}}{2}\right)^{1/2}\mathrm{U} \tag{20}$$

U and *f* are the mean velocity and friction factor, respectively.

2.4.4. Heat Transfer Enhancement and Performance Evaluation Criteria

The heat transfer enhancement ratio (ER) is calculated as below, which is the ratio of the Nusselt number in an enhanced (dimpled tube) case to the Nusselt number in the base case (plain tube) (Kukulka et al., 2013):

$$ER = \frac{\mathrm{Nu_{dimple}}}{\mathrm{Nu_{plain}}} \tag{21}$$

Performance evaluation criteria (PEC) proposed by Gee and Webb (1980) to investigate the overall performance of heat transfer and pressure drop can be calculated as follows:

$$PEC = \frac{Nu_d/Nu_p}{(\frac{f_d}{f_p})^{1/3}} \tag{22}$$

2.4.5. Entrance Length

To insure the full development of the flow field hydrodynamically and thermally before entering the tube being tested, it is important to calculate the necessary entrance length for laminar and turbulent flows.

In the case of laminar flow, the hydrodynamic and thermal entrance lengths can be calculated thus (Cengel, 2014):

$$L_{h,laminar} \approx 0.05ReD \tag{23}$$

$$L_{t,laminar} \approx 0.05RePrD \tag{24}$$

where *D* is the tube diameter with *h* and *t* donating hydrodynamic and thermal lengths, respectively.

Prandtl number

$$Pr = \frac{\mu c_p}{k} \tag{25}$$

For the turbulent flow, the entrance length can be calculated via (Cengel, 2014):

$$L_{h,turbulent} \approx L_{t,turbulent} = 10D \tag{26}$$

2.5. TURBULENCE MODELING

The flow phenomena in the current study is turbulent. Based on that, approaching the solution of the flow by choosing the most reliable and suitable turbulence model among the models available in the literature, such as the k-ε, k-ω and Reynolds stress models. According to the literature (Alshehri et al., 2020), the most common turbulence model used for heat exchanger analysis is the realizable k-ε and SST k-ω due to their ability to be highly predictive of the turbulent flow characteristic under the boundary conditions specified for the present physical problem. In this study, realizable k-ε is the turbulence model that is adopted to carry the solutions since it has the capability of resolving near wall flows and provides reliable results in comparison to other models.

2.5.1. Standard k-ε Model

The basic and most used model in the turbulent family is the standard k-ε model, the history of which goes back to 1972 when Launder and Spalding (1972) developed it to meet the necessary needs of solving and predicting the characteristics of fully developed turbulent flow. The turbulent kinetic energy k and dissipation rate ϵ are simply solved using the transport formulas as follows:

$$\frac{\partial(\rho k u_i)}{\partial x_i} = \frac{\partial}{\partial x_i}\left[\left(\mu + \frac{\mu_t}{\sigma_k}\right)\frac{\partial k}{\partial x_i}\right] + G_k - \rho\epsilon - Y_M \tag{27}$$

$$\frac{\partial(\rho \epsilon u_i)}{\partial x_i} = \frac{\partial}{\partial x_i}\left[\left(\mu + \frac{\mu_t}{\sigma_\epsilon}\right)\frac{\partial \epsilon}{\partial x_i}\right] + C_{1\epsilon}\frac{\epsilon}{k}G_k - \rho C_{2\epsilon}\frac{\epsilon^2}{k} \tag{28}$$

Where G_k and Y_M are the generation of turbulent kinetic energy due to the mean velocity gradient and the contribution of fluctuating dilatation in compressible turbulence to the overall dissipation rate, respectively.

The eddy viscosity is calculated thus:

$$\mu_t = \rho C_\mu \frac{k^2}{\epsilon}$$

The constants are taken as $C_\mu = 0.09$, $C_{1\epsilon} = 1.44$, $C_{2\epsilon} = 1.92$, $\sigma_k = 1.0$ and $\sigma_\epsilon = 1.3$ (ANSYS, 2009)

2.5.2. Realizable k-ε Model

The excellence of the realizable k-ε model in comparison with others in the k-ε family is due to the formulation containing improved terms of the turbulent viscosity

and modern transport equations for the dissipation rate. These two improvements provide accurate predictions to solve physical problems involving boundary layers within a strong adverse pressure gradient, separation and recirculation (ANSYS, 2009).

For turbulent kinetic energy *k*, the transport equation is modified as:

$$\frac{\partial(\rho k u_i)}{\partial x_i} = \frac{\partial}{\partial x_i}\left[\left(\mu + \frac{\mu_t}{\sigma_k}\right)\frac{\partial k}{\partial x_i}\right] + G_k - \rho\epsilon - Y_M \tag{29}$$

G_k, Y_M and σ_k represent the generation of turbulent kinetic energy due to the mean velocity gradient, the contribution of fluctuating dilatation in compressible turbulence to overall dissipation rate and a turbulent Prandtl number for *k*, respectively.

In addition to the transport equation related to energy dissipation (ϵ), the equation is written as

$$\frac{\partial(\rho\epsilon u_i)}{\partial x_i} = \frac{\partial}{\partial x_i}\left[\left(\mu + \frac{\mu_t}{\sigma_\epsilon}\right)\frac{\partial \epsilon}{\partial x_i}\right] + \rho C_1 S\epsilon - \rho C_2 \frac{\epsilon^2}{k+\sqrt{\nu\epsilon}} \tag{30}$$

$$\mathrm{C_1} = \max\left[0.43, \frac{\eta}{\eta + 5}\right]$$

$$\eta = \mathrm{S}\frac{\mathrm{k}}{\epsilon}$$

$$\mathrm{S} = \sqrt{2\mathrm{S_{ij}}\mathrm{S_{ij}}}$$

C_2 and $C_{1\epsilon}$ are constants.

Hence, $C_2 = 1.9$, $C_{1\epsilon}$, $= 1.44$, $\sigma_k = 1.0$ and $\sigma_\epsilon = 1.2$.

The eddy viscosity μ_t is calculated as

$$\mu_t = \rho \mathrm{C_\eta} \frac{\mathrm{k}^2}{\epsilon}$$

C_η is calculated as

$$\mathrm{C_\eta} = \frac{1}{\mathrm{A_0} + \mathrm{A_s}\frac{\mathrm{kU^*}}{\epsilon}}$$

where

$$U^* = \sqrt{S_{ij}S_{ij} + \widetilde{\Omega}_{ij}\widetilde{\Omega}_{ij}}$$

$$A_0 = 4.04, \qquad A_s = \sqrt{6}\cos\emptyset$$

Since $\emptyset = 3\cos^{-1}\sqrt{6W}$ and $W = \frac{S_{ij}S_{ik}S_{ki}}{\tilde{S}^3}$, $\quad \tilde{S} = \sqrt{S_{ij}S_{ij}}$, $\quad S_{ij} = 0.5\left(\frac{\partial u_j}{\partial x_i} + \frac{\partial u_i}{\partial x_j}\right)$

2.5.3. The k-ω SST Model

The k-ω SST model is considered to be the newest turbulent model being used and preferred in many turbulent flow studies based on it is advantages in comparison to k-ε models. This model was developed in the mid-1990s by Menter (1994) to resolve and improve the accuracy of solving and capturing the boundary layer near the walls, for which it deserves its good reputation among researchers and industries. The shear stress transport model uses the following equation to solve the *k* and *ω* terms:

$$\frac{\partial(\rho k u_i)}{\partial x_i} = \frac{\partial}{\partial x_i}\left[\left(\mu + \frac{\mu_t}{\sigma_k}\right)\frac{\partial k}{\partial x_i}\right] + G_k - Y_k \tag{31}$$

$$\frac{\partial(\rho \omega u_i)}{\partial x_i} = \frac{\partial}{\partial x_i}\left[\left(\mu + \frac{\mu_t}{\sigma_\omega}\right)\frac{\partial k}{\partial x_i}\right] + \widehat{G_\omega} - Y_\omega + D_\omega \tag{32}$$

where $\widehat{G_\omega}$, Y_ω and D_ω are the production of the turbulence kinetic energy, dissipation of turbulence kinetic energy and cross diffusion, respectively.

CHAPTER 3

NUMERICAL ANALYSIS

3.1. PHYSICAL MODEL

In the present chapter, details of the numerical analysis applied in the current study are described. ANSYS Fluent software was utilized to solve the nonlinear governing equations presented in the previous chapter for the described physical problem of steady incompressible turbulent flow and heat transfer in a capsule dimpled tube (CDT) with a nanofluid as the working fluid.

To investigate the enhancement performance of the different depths of capsule dimples and different volume concentrations of nanofluids on the heat transfer and pressure drop, the realizable k-ε model with enhanced wall treatment was implemented. The thermal properties of the working fluid are considered to be constant while nanoparticle concentration is assumed to be homogeneous. Since the nanoparticle concentration is low, the flow is considered to be a single phase flow.

As shown in Figure 3.1, the physical geometry considered in this analysis is divided into two regions. A dimpled tube region 440 mm in length and entrance length to ensure the full development of the flow entering the dimpled tube region. Hence, a 200 mm length is added for this reason and the tube diameter is fixed to 18 mm.

It is worth noting that, the inline orientation of the dimples along the tube surface allows the consideration of the flow domain as a quarter axi-symmetric domain. Hence the computations are performed only for one quarter, as illustrated in Figure 3.1. The advantages of this approach are practical meshing and the need for less computational time. In the current study, water and nanofluid at different volume concentrations (1%, 2% and 3%) are used as the working fluid and the inlet temperature of the working fluid is prescribed as 293°K.

This numerical study has a varying number of dimple geometrical parameters (dimple depth of 1 mm, 1.5 mm, 2 mm and 2.5 mm) and different nanoparticle

volumetric concentrations (1%, 2% and 3%) affecting the heat transfer between the fluid and the tube wall. The geometrical parameters of the dimples are shown in Figure 3.1 and their values considered in the study are given in Table 3.1.

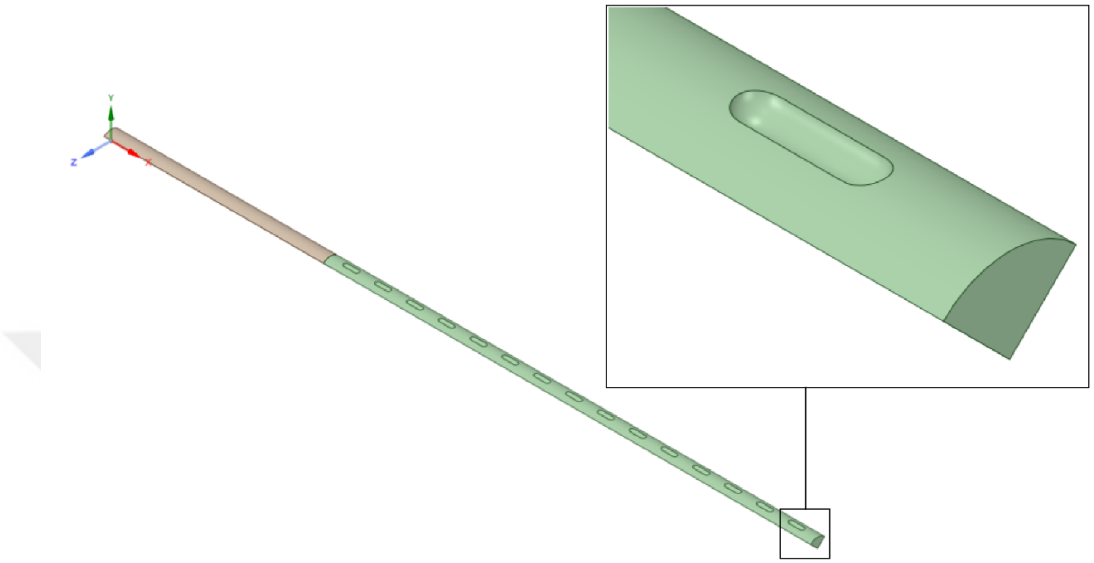

Figure 3.1 Quarter symmetrical section of a capsule dimple tube.

Table 3.1 Values of dimpled tube parameters considered in the study.

Tube Diameter D_t	18 mm
Dimpled Tube length L_d	440 mm
Dimple length d	12/13/14/15 mm
Pitch P	15 mm
Dimple Depth h	1/1.5/2/2.5 mm
Center to center length w	10 mm
Entrance Length	12,000 mm (Laminar) 200 mm (Turbulent)

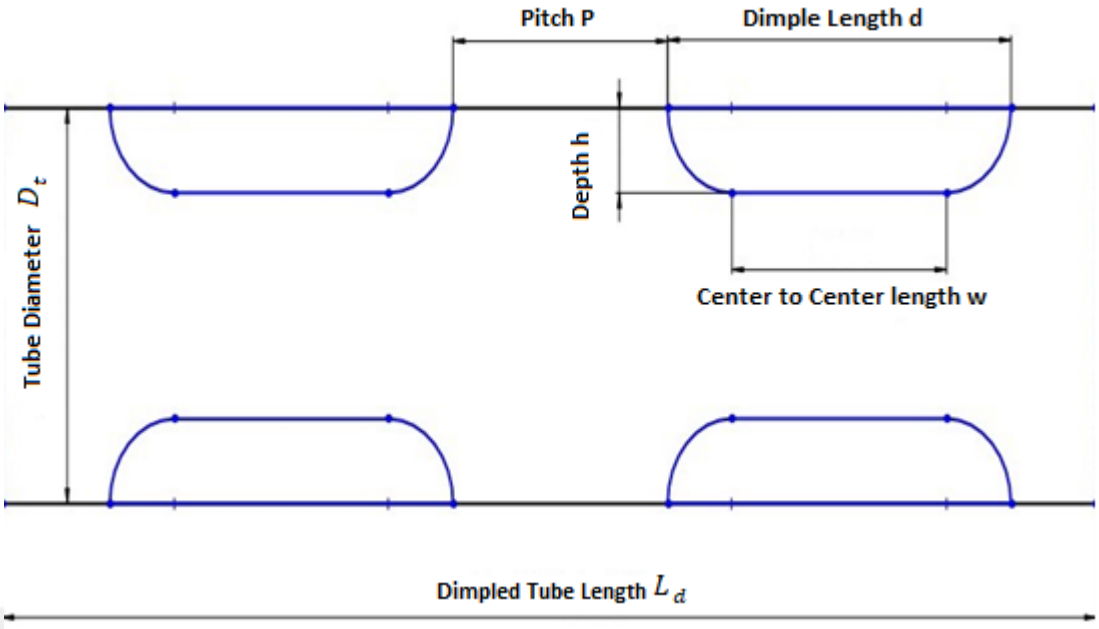

Figure 3.2 Schematic for the geometrical parameters of the dimpled tube.

The convergence residuals for all equation variables are set to $10e^{-06}$ and the number of iterations are 1,000 for all cases. The solution method was adopted for solving the pressure and velocity coupling via the Semi-Implicit Method for Pressure Linked Equations (SIMPLE) algorithm. Momentum and energy equations were solved by the second order upwind scheme.

3.2. MESH GENERATION

To insure the reliability and compatibility of the numerical analysis, a good computational mesh must be generated. Throughout this mesh generation, a 2-D plain tube and four row 3-D capsule dimpled tube (CDT) with different dimple depths are taken into consideration, which requires a fine quality mesh discretization for the flow domain. To resolve the sublayer regions developed near the tube wall, a fine mesh structure usually with $y^+ \cong 1$ must be implemented. The height of the wall adjacent cell can be calculated using Equations (9) and (10). The mesh structure adopted in the current study are hexahedral for the 2-D plain tube, as can be seen in Figure 3.3, and a tetrahedral structure for the 3-D CDT, as presented in Figure 3.4. The mesh utilized in this research was produced using the ANSYS 2020R1 meshing tool.

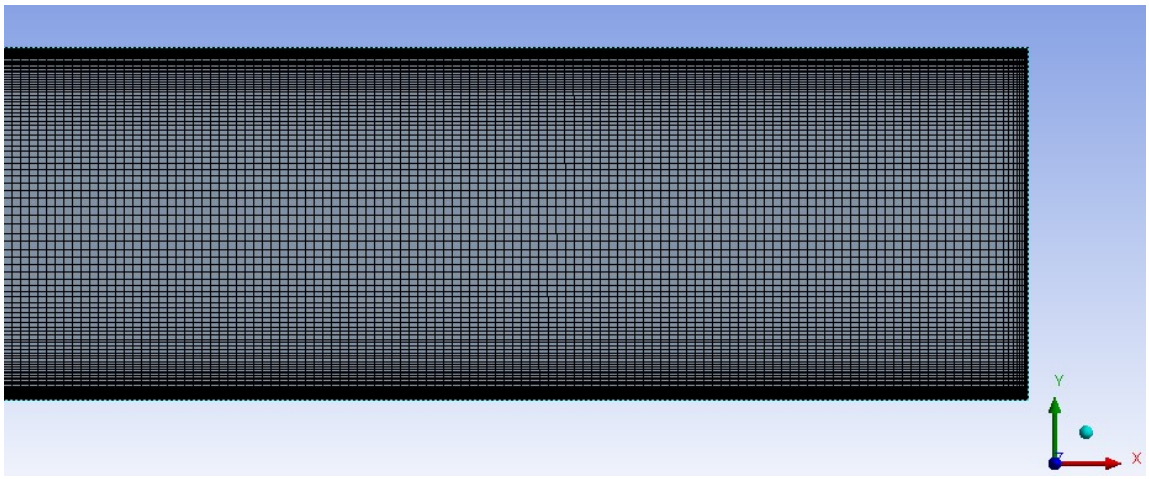

Figure 3.3 Mesh structure for 2-D plain tube**.**

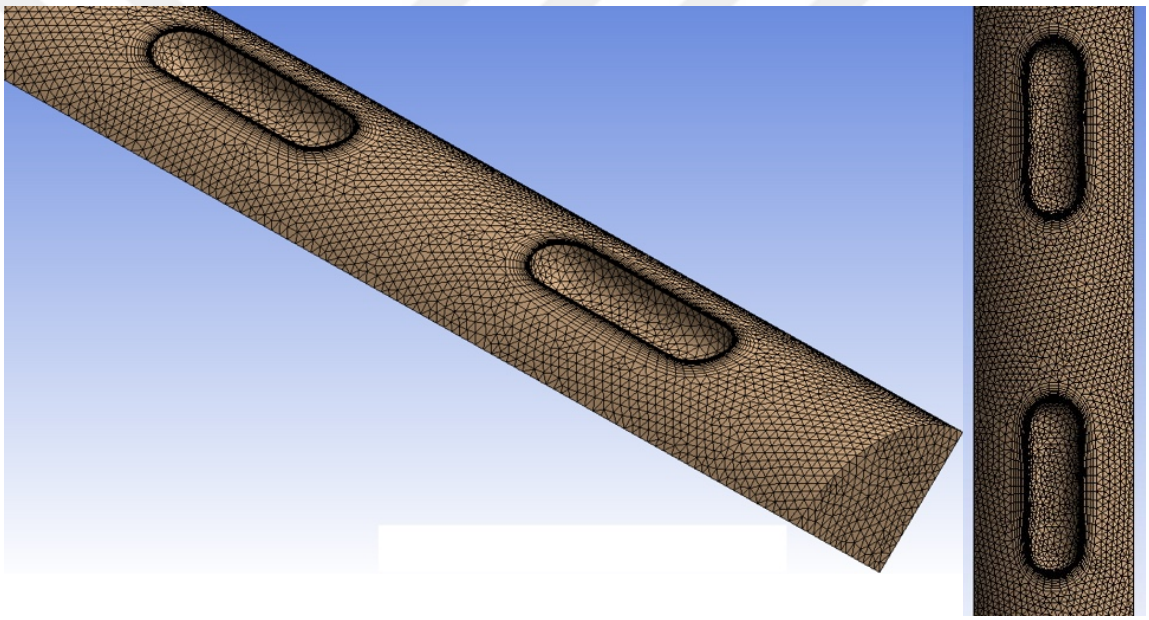

Figure 3.4 Mesh structure capsule dimpled tube.

3.3. BOUNDARY CONDITIONS

The solution of the nonlinear partial differential equations mentioned previously requires a proper definition of the boundary conditions related to the current physical problem. The Reynolds number at the inlet ranging from 2,000 to 14,000, where the temperature is kept at a constant 293°K temperature at the inlet. The thermophysical properties for both the water and Al_2O_3-water nanofluid are kept constant throughout the flow. The outlet pressure is constant and specified. A uniform heat flux over the dimpled pipe surface is applied. To be confident about the full development of the velocity entering the dimpled tube, a pre-specified entrance length

is selected as being 200 mm for the 3-D capsule dimple tube. For further illustration, Tables 3.2, 3.3 and 3.4 can be referred to below. Different cases of capsule dimple geometries and volumetric concentrations of nanoparticles in the base fluid are considered in this study. The boundary conditions illustrated in Figure 3.5 showed a uniform velocity at the inlet varying between 0.1 and 1.9 m/s^2 in both water and different concentrations of nanofluid and a constant heat flux of 10,000 W/m^2 along the dimpled tube surface.

Table 3.2 Boundary conditions considered for the numerical simulation.

Boundary	Type	Parameters
Tube Inlet	Reynolds Number	2,000-14,000
Tube Inlet	Temperature	T = 293°K
Tube Surface	Uniform Heat Flux	Q = 10000 W/m^2
Tube Outlet	Pressure Outlet	P_o = 0 Pa

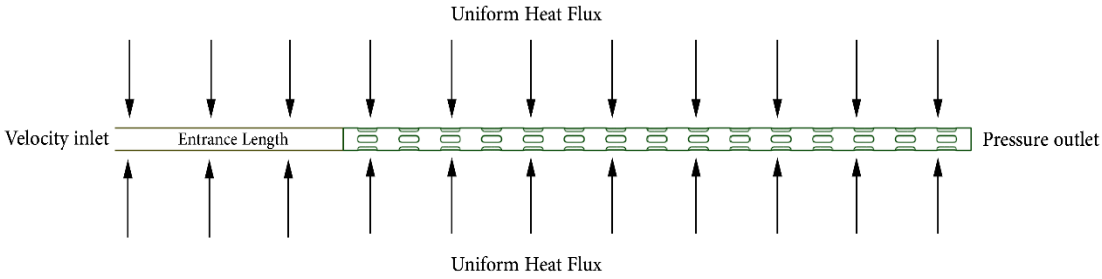

Figure 3.5 Boundary conditions

The thermophysical properties of the base fluid and nanoparticles are given in the table below (Minea, 2017)

Table 3.3 Thermophysical properties of base fluid and nanoparticles

Material	Specific heat (J.kg^{-1}.K)	Density (kg/m^3)	Thermal conductivity (W.m^{-1}.K)	μ (Pa.s)
Al_2O_3	765	3970	40	-
Water	4,181	996.5	0.613	0.001

Table 3.4 Thermophysical properties of Al_2O_3-Water nanofluid at different nanoparticle volume concentrations.

Volume Concentration (%)	ρ (kg/m^3)	μ (Pa.s)	c_p (J.kg^{-1}.K)	k (W.m^{-1}.K)
1	1,026.235	0.00144449	4,048.85171	0.6307
2	1,055.97	0.00199576	3,924.15	0.6488
3	1,085.705	0.002654	3,806.271	0.667

3.4. MESH INDEPENDENCE STUDY

To verify the validity of the simulation results and to keep the computational costs as low as possible, the tube was studied using the realizable k-ε turbulence model at constant Reynolds numbers (14,000) with various mesh element numbers. The average Nusselt number obtained with different meshes for the case of a 2-D plain tube as shown in Figure 3.6 and in Table 3.5 gives the mesh studies of 3-D capsule dimple tubes at different dimple depths. The meshes utilized in this research were produced using the meshing tool in ANSYS 20R1. The mesh convergence analysis was performed by generating ten different meshes in the case of the 2-D plain tube to evaluate how the mesh quality impacts simulation outcomes. Figure 3.6 illustrates that the simulation accuracy is reliant on the number of mesh elements used. The mesh elements created have near wall resolution of $y^+ \cong 1$, and by utilizing the enhanced wall treatment method (which has an important role in capturing the near wall boundary layers via realizable k-ε turbulence model) to minimize any bad outcomes that may occur and increase the results prediction accuracy. Hence, the number of mesh elements employed with different depths of capsule dimpled tube geometries include 3.1, 2.6, 3.1, and 2.3 million mesh elements for 1 mm, 1.5 mm, 2 mm and 2.5 mm dimple depths, respectively, which can be seen in Table 3.5. Then for the plain tube, 200,000 is selected.

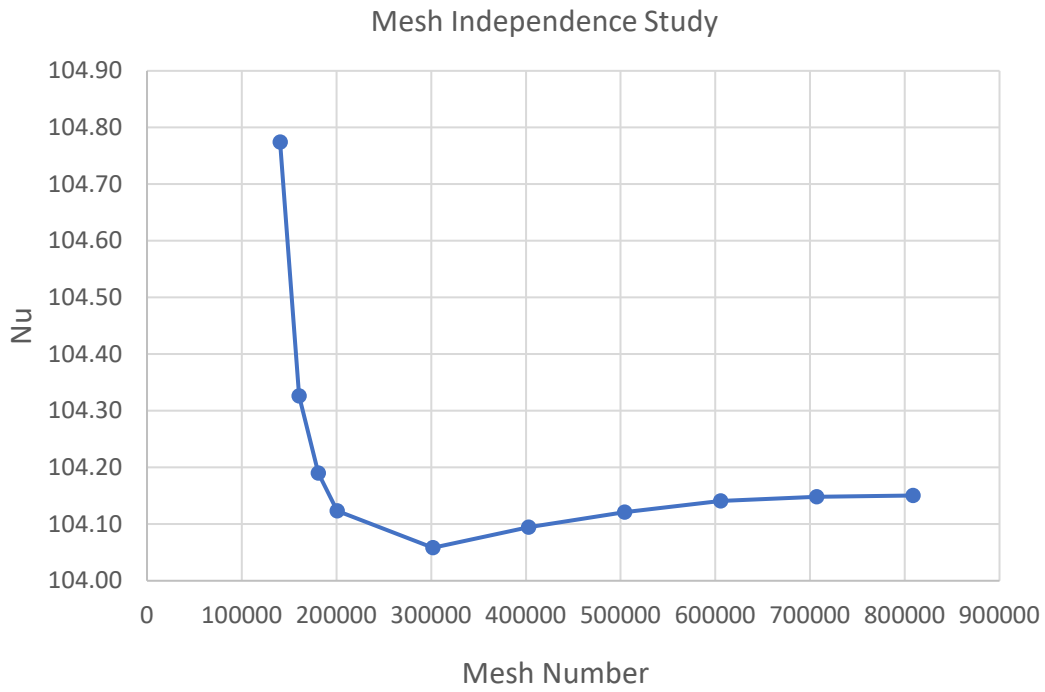

Figure 3.6 Variation of Nusselt number with mesh number for 2-D plain tube.

Table 3.5 Mesh study on CDT for 1 mm, 1.5 mm, 2 mm and 2.5 mm depths.

Mesh (Million)	Nu for 1 mm depth
2.6	124.51
2.8	124.18
3	125.09
3.1	124.82

Mesh (Million)	Nu for 1.5 mm depth
2.2	142.71
2.6	143.51
2.9	143.27
3.4	143.92

Mesh (Million)	Nu for 2 mm depth
1.6	151.45
1.9	152.13
2.4	153.52
2.7	154.36

Mesh (Million)	Nu for 2.5 mm depth
1.8	162.97
2.3	162.93
2.7	165.33
3.3	166.25

3.5. COMPARISON OF TURBULENCE MODELS

To assess the accuracy of the CFD solution, a sequential study was conducted using the turbulence models (realizable k-ε, standard k-ε and the SST k-ω) with 200,000 sized mesh elements. The Nusselt numbers are obtained with different models and compared to the correlation, as plotted in Figure 3.7. Similarly, the friction factors are plotted in Figure 3.8. As seen in Figure 3.8, the friction factor for the realizable k-ε model has a better approach than the other models for all Reynolds numbers being considered. From the turbulence models studied, it can be observed that the realizable

k-ε turbulence model performs better for the Nusselt numbers and the friction factor than the standard k-ε model and SST k-ω, as shown in Figures 3.7 and 3.8, respectively. Based on that, the realizable k-ε turbulence model is selected.

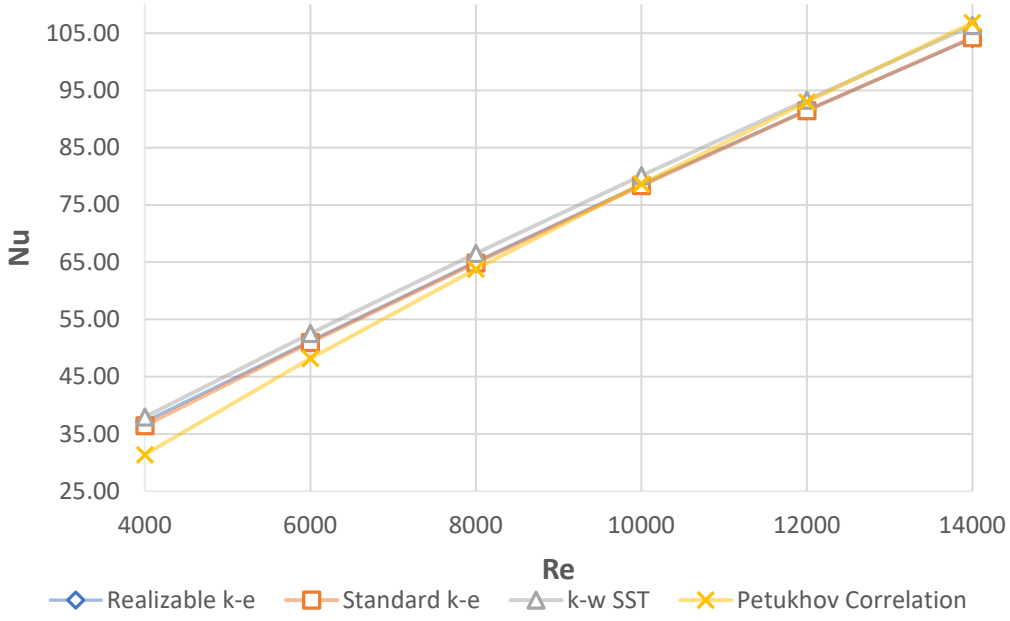

Figure 3.7 Nusselt number comparison between turbulence models and the Petukhov correlation.

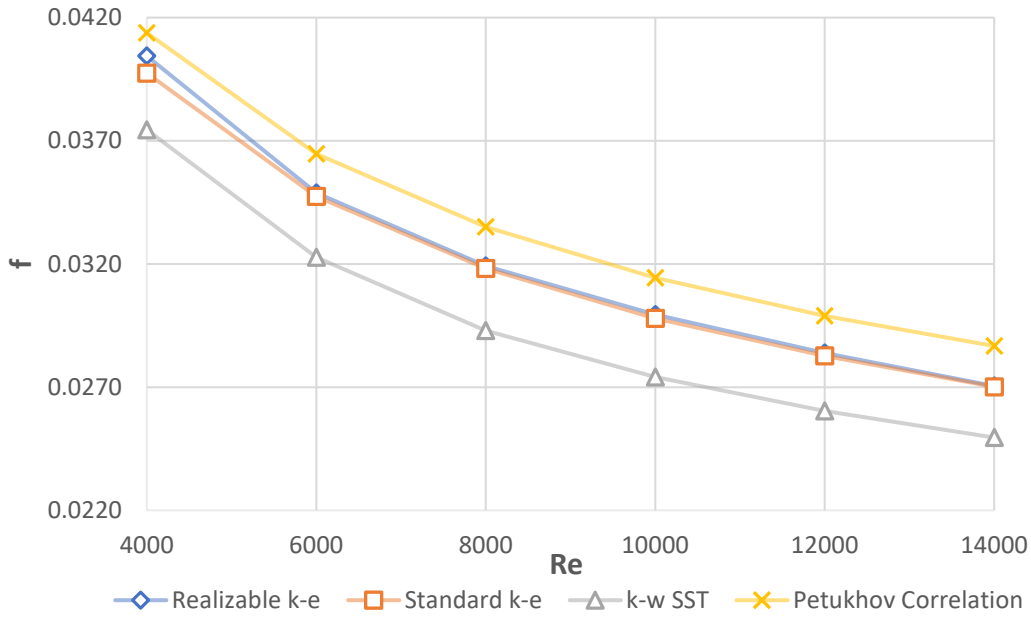

Figure 3.8 Friction factor comparison between turbulence models and Petukhov correlation.

3.6. VALIDATION OF NUMERICAL RESULTS

To validate the numerical methods used in the present study, validation studies are performed for three different cases:

1. Water flow in a plain tube for the current study
2. Nanofluid flow in a plain tube
3. Water flow in a dimpled tube

3.6.1. Verification Study for Water Flow in Plain Tubes for the Present Studied Geometry

Figure 3.9 illustrates a Nusselt Number Comparison between a plain tube (the present study) and computed correlation (Petukhov Correlation) for the turbulent region. For the laminar region, the Nusselt number is 4.29, which is acceptable when compared with the literature (Cengel, 2014). The simulated Nu demonstrates a conformity to the other computed Nu within the acceptable range of errors. The maximum is 18% and the minimum is 0.1%.

For the case of fully developing laminar flow in a circular tube with a uniform surface heat flux, the Nusselt number is constant.

$$\mathrm{Nu} = \frac{hD}{k} = 4.36$$

For turbulent flow, the Petukhov Correlation is used to compute the Nusselt number:

$$\mathrm{Nu} = \frac{\left(\frac{\mathrm{f}}{8}\right)(\mathrm{Re} - 1000)\mathrm{Pr}}{1 + 12.7\left(\frac{\mathrm{f}}{8}\right)^{0.5}(\mathrm{Pr}^{\frac{2}{3}} - 1)}$$

This correlation is valid for the ranges of $(3{,}000 < \mathrm{Re} < 5 \times 10^6)$ and $(0.5 \leq \mathrm{Pr} \leq 2{,}000)$.

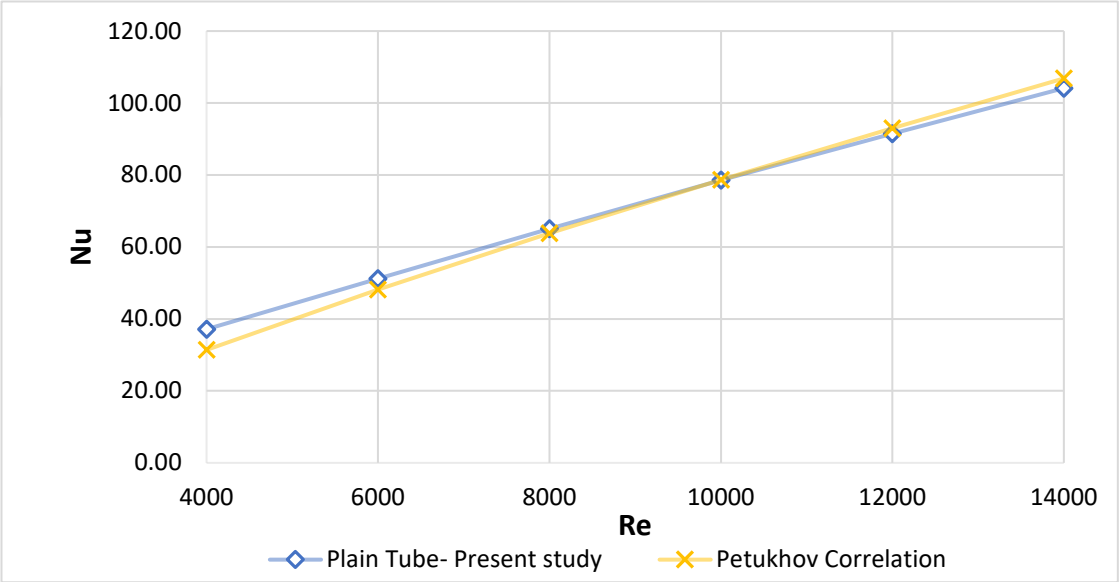

Figure 3.9 Comparison of numerically calculated Nusselt numbers with Petukhov correlation in plain tube.

The friction factor estimated from the plain tube (present study) shows agreement with the computed correlation (Petukhov correlation), as seen in Figure 3.10. The errors fall within the acceptable range of values.

The Petukhov Correlation for the friction factor in the case of fully develop turbulent flow is:

$$\mathrm{f} = (0.790\ \ln\mathrm{Re} - 1.64)^{-2}$$

Working range is $(3000 < \mathrm{Re} < 5 \times 10^6)$.

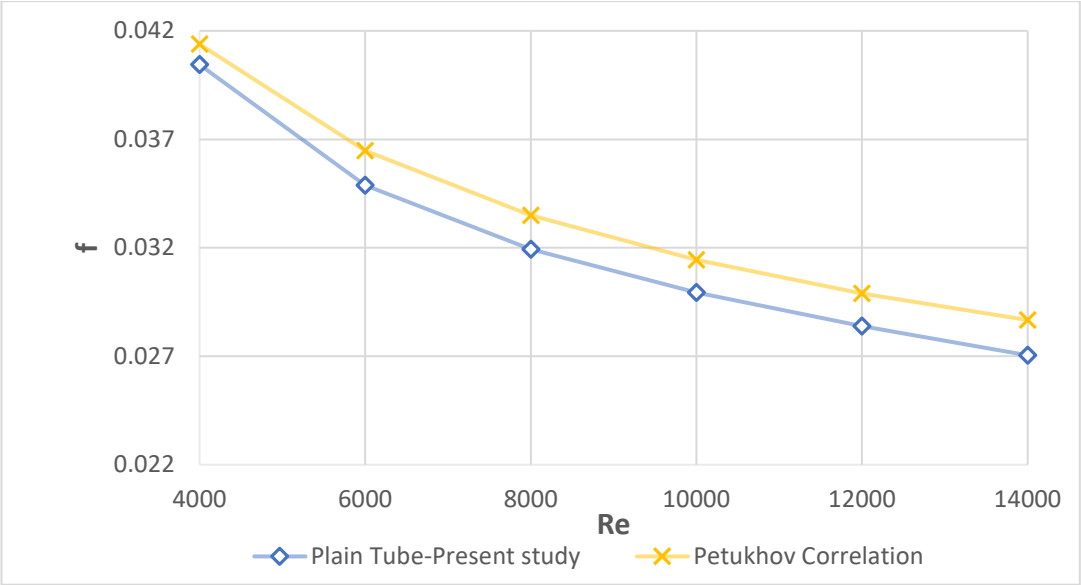

Figure 3.10 Comparison of numerically calculated friction factors with Petukhov correlation in plain tube.

3.6.2. Verification Study for Single Phase Water and Nanofluid Flow in a Plain Tube

A validation study was carried out based on single phase water flow and nanofluid flow results of a study by Alshehri et al. (2020). In this study, as the base fluid, water and ethylene glycol hybrid fluid was used. The nanoparticles Al_2O_3 and TiO_2 were added to the hybrid fluid. A uniform heat flux was applied through the surface of the pipe. The Reynolds number ranged between 7,800 and 22,000. The thermophysical properties of both water and the hybrid nanofluid at certain nanoparticle concentrations are given in the table below (Alshehri et al, 2020):

Table 3.6 Thermophysical properties for both base fluid and nanofluid.

Fluid Type	**ρ (kg/m^3)**	**μ (Pa.s)**	**c_p (J kg^{-1}.K)**	**k (W.m^{-1}.K)**
Water	998.2	0.000998	4,182	0.597
Water/ethylene glycol 2.5% Al_2O_3-1.5% TiO_2 Hybrid Nanofluid	1166.6	0.0037	3241.5	0.4969

A uniform heat flux was applied along the pipe surface. At the inlet, uniform velocity and temperature were considered. For simulations, the realizable k-ε

turbulence model was used with a 900K mesh. From the simulation results, the Nusselt number and friction factor were calculated and compared with values given by Alshehri et al. (2020) and correlations suggested by Nutter-Roase (1972) for the Nusselt number and Petukhov equation (1970) for the friction factor.

Figures 3.11 and 3.12 show the Nusselt number calculated from the simulation results for single phase water and hybrid-nanofluid being compared with the results calculated by the Nutter-Roase correlation and numerical results by Alshehri et al. (2020) for different Reynolds numbers. Figure 3.13 presents a comparison between the friction factor of the numerical results for the hybrid nanofluid and the correlation calculated by Petukhov (1970).

It can be observed form Figure 3.11 clear evidence of agreement between the numerical results extracted from the simulation to the correlation based on results from previously performed experiments with a maximum of 11.5% and minimum of 7.4% errors.

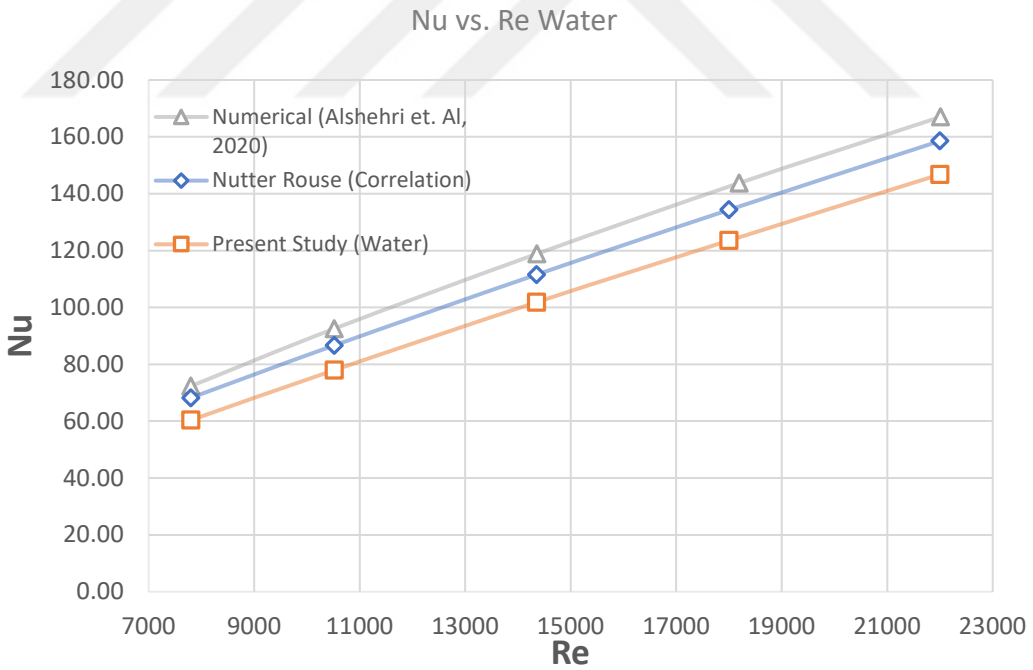

Figure 3.11 Comparison of numerical Nusselt numbers with correlations for flow of water in plain tubes.

Figure 3.10 shows a comparison of the numerical Nusselt number with the Nuttor-Rouse correlation and numerical results given by Alshehri et al. (2020). The

accuracy of agreement is improved by increasing Re and the enhancement of the Nusselt number in comparison to Figure 3.12 due to the improvement of thermophysical properties of the hybrid-nanofluid 2.5% Al_2O_3 and 1.5% TiO_2. The maximum error for this case is 4.8% and the minimum is 1.2%.

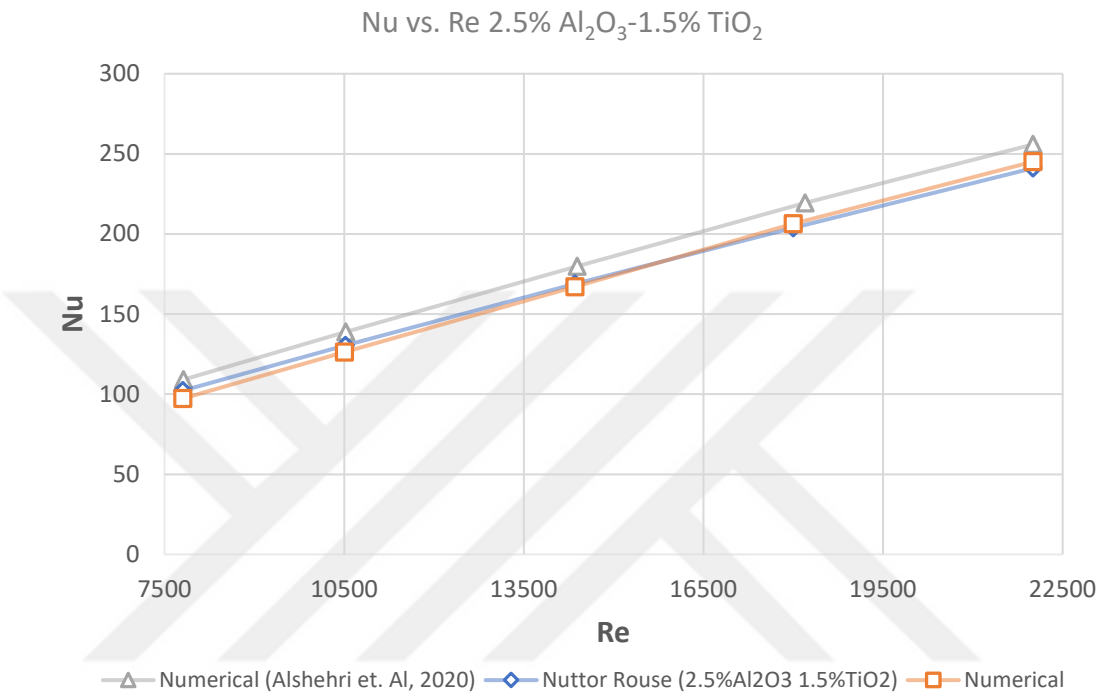

Figure 3.12 Comparison of numerical Nusselt numbers with correlations, hybrid-nanofluid

Similarly, in Figure 3.13, it is clear that the friction factor for the numerical results shows an agreement with the friction factors calculated by Petukhov.

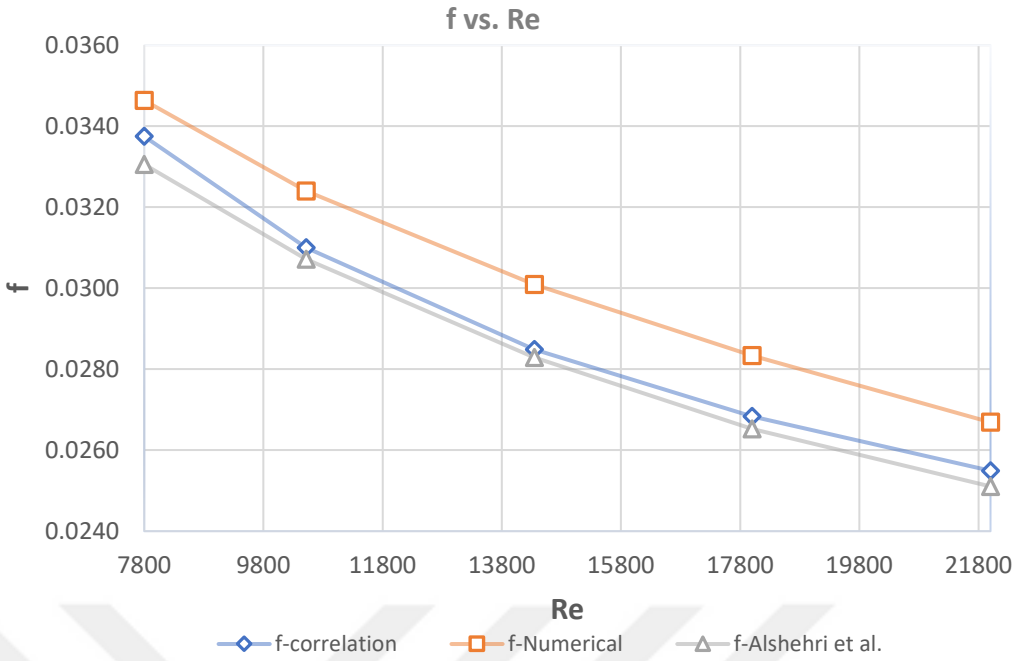

Figure 3.13 Comparison of numerical friction factors with correlations, hybrid nanofluid.

The figures illustrated previously show an agreement between the numerical results of the Nusselt numbers and the friction factor associated with errors of ±10% compared to the experimental correlations, which is considered to be acceptable (Ming et al., 2016).

3.6.3. Verification Study for Water Flow in Dimpled Tubes

For further demonstration of the validity of the results regarding the dimpled tube, verification based on the study by Sabir et al. (2020) on an ellipsoidal dimpled tube was considered. The geometrical characteristic for the tube and the dimples are given in Table 3.7 below:

Table 3.7 Geometrical characteristics.

Tube Diameter [mm]	Dimple Diameter [mm]	Depth [mm]	Pitch [mm]	Tube Length [mm]	Entrance Length [mm]
17.272	3.89506	1.1686	10	120	370

An ellipsoidal dimple tube is considered in this study with boundary conditions such that heat flux is constant along the tube surface. A uniform velocity isconsidered at the inlet and the pressure at the outlet is set to be zero. Tables 3.8 and 3.9 provide further illustration on the boundary conditions used in this study.

Table 3.8 Simulation boundary conditions for validation.

Reynolds Number	4,500-15,000
Temperature Inlet	305.5°K
Outlet	Pressure Outlet
Heated Wall (dimpled surface)	10,000 W/m^2
Working Fluid	Water

Table 3.9 Working fluid thermal properties.

Fluid Type	**ρ (kg/m^3)**	**μ (Pa.s)**	**c_p (J.kg^{-1}.K)**	**k (W.m^{-1}.K)**
Water	994.57	0.00075407	4,020.83	0.62215

The ANSYS Fluent software package was used to perform this validation for the mesh number of 1,000,000 and the realizable k ε turbulent model was chosen, which was found to provide far more accurate results in terms of the Nusselt number and friction factor compared to the SST k-ω model (Ming et. al., 2016). It is important to mention that the compared Nusselt numbers and friction factors are calculated from the correlations proposed by Sabir et al. (2020), which are based on ellipsoidal angular orientation α (for the current study, α = 0) and the Reynolds number (Re). The correlations are as follows:

$$\mathrm{Nu} = aRe^{b(1+0.3\propto/2\pi)}$$

$$(a = -0.0006617 \propto + 0.1347\ b = 0.00051111 \propto + 0.7412)$$

$$fr = [a \ln\left(\mathrm{Re} + \frac{\propto}{2\pi}\right) + b]^{-3/2}$$

$$(a = -0.0079747 \propto + 1.2462, b = 0.059878 \propto - 5.3636)$$

where α and Re are in the range of:

$$0°$$

$$0° \leq \alpha \leq 90°$$

$$2{,}300 \leq Re \leq 15{,}000$$

These correlations have an error division less than 20% for the Nusselt number and less than 25% for the friction factor in comparison to the numerical results obtained within the same research paper.

Figures 3.14 and 3.15 present a numerical comparison of Nusselt numbers and friction factors with the results of the numerical study conducted by Sabir et al. (2020) in addition to the correlation proposed by Sabir et al. (2020).

The following figures illustrate the Nu and f vs. Re for the ellipse dimple tube.

Figure 3.14 shows all three Nusselt numbers related to the simulated study, calculated correlation and numerical data provided by the validated research paper. The simulated Nu shows an agreement with the other calculated Nu within the acceptable range of errors.

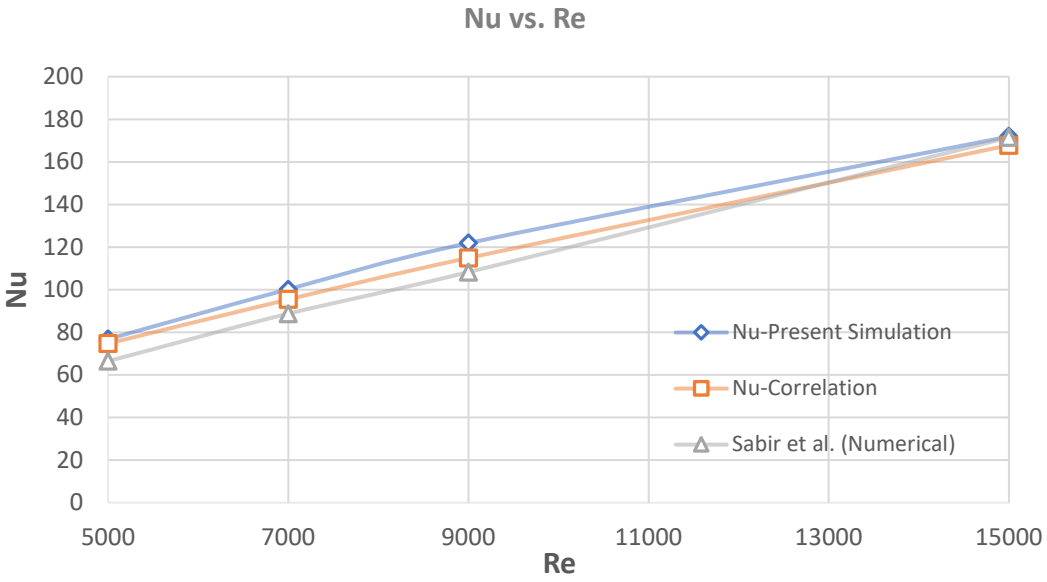

Figure 3.14 Comparison of Nusselt numbers calculated from simulations with Nusselt number correlations and numerical Nusselt numbers by Sabir et al. for ellipsoidal dimpled tube.

The friction factor calculated from the simulation showed an agreement, as seen in Figure 3.15. The errors affecting the results that would be due to some numerical approximations and assumptions are about 10 to 20% lie within the acceptable range (Sabir et al., 2020)

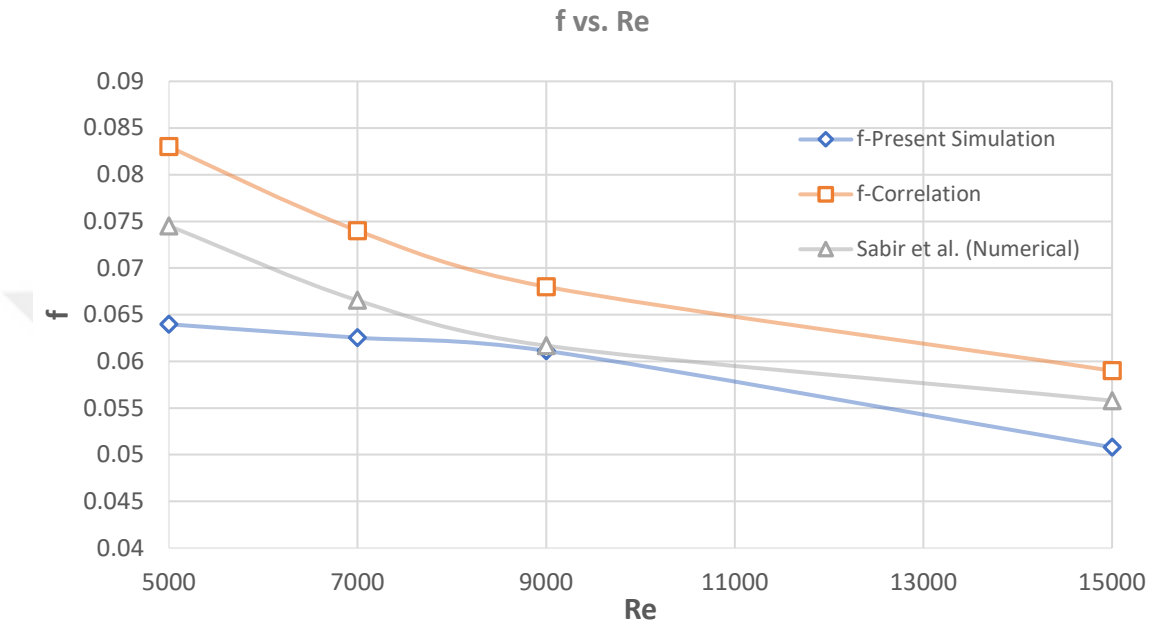

Figure 3.15 Comparison of friction factor calculated from simulations with friction factor correlations and numerical friction factors by Sabir et al. for ellipsoidal dimpled tube.

CHAPTER 4

RESULTS AND DISCUSSION

Throughout this chapter, detailed results are given on the thermal and hydrodynamic improvements caused by geometrical modifications to the tube surface in which capsule dimples are introduced, additionally adopting Al_2O_3-Water nanofluid at different volume concentrations as the heat transfer fluid. A detailed discussion is presented on each finding.

In the study, the flow of nanofluid in a capsule dimpled tube was simulated and the results were compared with the flow in a plain tube. The simulations are performed with different dimple depths (1 mm, 1.5 mm, 2 mm, and 2.5 mm), different volume concentrations (1%, 2% and 3%) and Reynolds numbers starting in laminar flow from 2,000 to transition at 4,000 and further for turbulent flow in the Reynolds number range of 6,000-14,000. The effects of these parameters on the Nusselt number, friction factor and performance evaluation criteria are investigated.

4.1. FLOW FIELD

Figure 4.1 presents the flow velocity distribution for a plain tube and dimpled tube with water and 2% nanofluid. It is clear from the figures that the velocities are varying along the dimpled tube. The flow enters as a fully developed flow and start changing when reaching the dimpled sections and as a result, the velocity increases rapidly then decreases after passing the dimpled sections. Moreover, the area behind each dimple shows a considerable decrease in velocity, which will lead to a sudden pressure drop causing vortices to develop in those areas, as seen in Figure 4.2.

Figure 4.3 shows the pressure gradient within the dimpled tube (water and 2% nanofluid) compared to the plain tube. As expected, the pressure drops in the dimpled sections and then increases afterward. This behavior causes an increase in the friction factor and pressure drop along the dimpled tube and it is highly affected by the depth

of the dimples. Due to the elevated velocity in the dimpled tube with the nanofluid, the pressure drop along the tube is higher than the dimpled tube with only water.

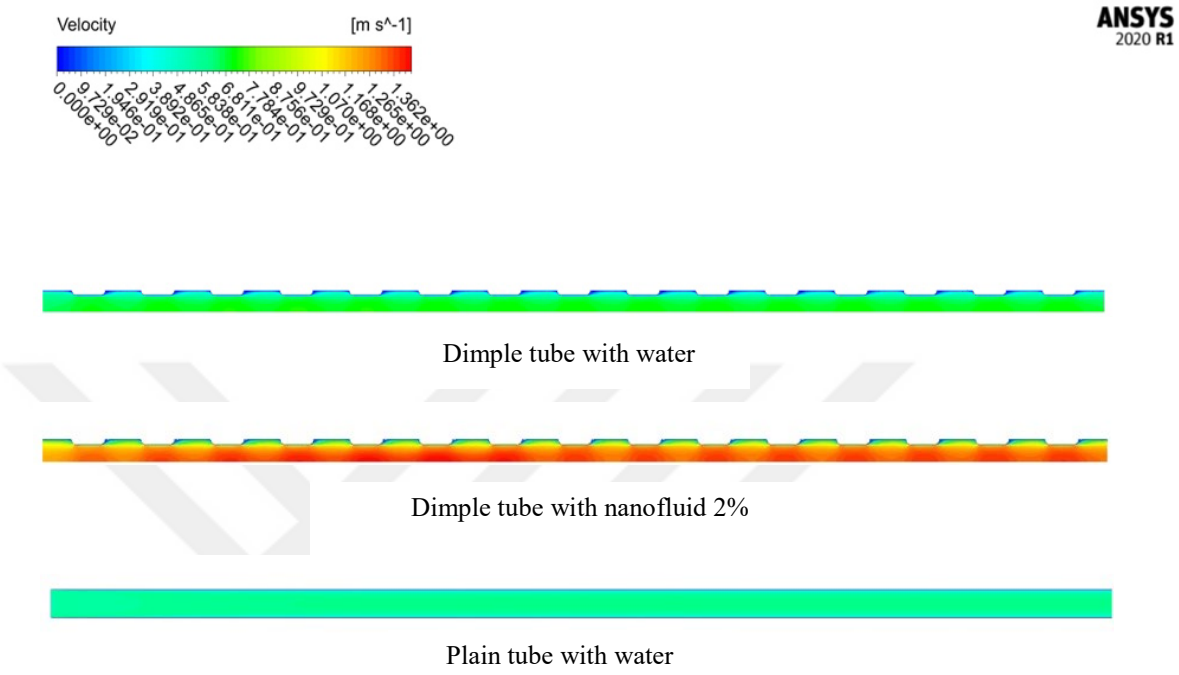

Figure 4.1 Velocity contours for dimpled tube with water, dimpled tube with 2% nanofluid and plain tube with water.

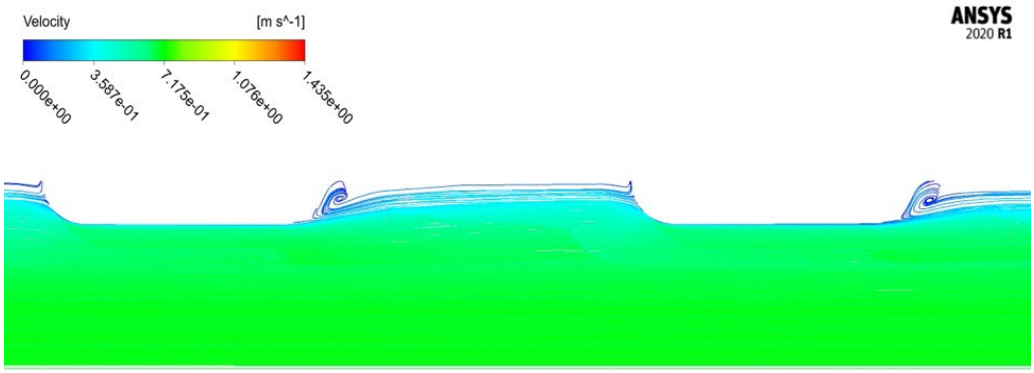

Dimple tube with water

Dimple tube with nanofluid 2%

Figure 4.2 Streamline contours for dimpled tube with water and dimpled tube with 2% nanofluid.

Dimple tube with water

Dimple tube with nanofluid 2%

Plain tube with water

Figure 4.3 Pressure contours for dimpled tube with water, dimpled tube with 2% nanofluid and plain tube with water.

4.2 EFFECT OF CAPSULE DIMPLED TUBES ON HEAT TRANSFER PERFORMANCE

The phenomenon of convective heat transfer is highly influenced by geometrical modifications such as dimples in the inner surface of the tube. Such effects are studied and presented in graphs for better visualization and understanding in this analysis.

In Figure 4.4, a comparison of Nu between a plain tube and a capsule dimpled tube (CDT) at different dimple depths for water as the working fluid can be seen. The figure presents the effects of a CDT at different dimple depths and various Reynolds numbers on the Nusselt number variation.

One can observe from Figure 4.4 that increasing the Reynolds number along with capsule dimple depth causes the Nusselt number to increase compared to the plain tube. The increasing in Nu in the laminar (Re = 2000) region between the plain tube and CDTs are significantly high; however, between the different depths of CDT, the increase is relatively low.

For the transitional region (Re = 4,000), the increase in all dimpled tubes are obvious in relation to the plain tube seen in Figure 4.1. Lastly, in turbulent regions, a linear pattern is observed when the Nusselt number increases.

Among all the studied dimpled tubes at different flow velocities, the 2.5 mm dimple depth tube at Re = 14,000 shows the maximum rise in the Nu number. The opposite trend is found in 1 mm dimple depth at Re = 2,000, excluding the plain tube.

For the Laminar region of the Reynolds number of 2,000, increasing the Re along with dimple depths causes the Nu to increase rapidly. The presence of dimples in a tube surface affects the flow domain by generating vortices which disturb the flow and allow the flow to reach a turbulent state even at lower Reynolds numbers where the flow is considered to be laminar in a plain tube. Increasing the dimple depth can increase the tube surface area accordingly and in contrast, allow the convective heat transfer to occur far more efficiently, thereby increasing the Nusselt number (Firoozi, 2020). Additionally, the disturbance in the laminar sublayer of the boundary layer caused by the presence of dimples increases as dimple depth increases (Suresh et al., 2011).

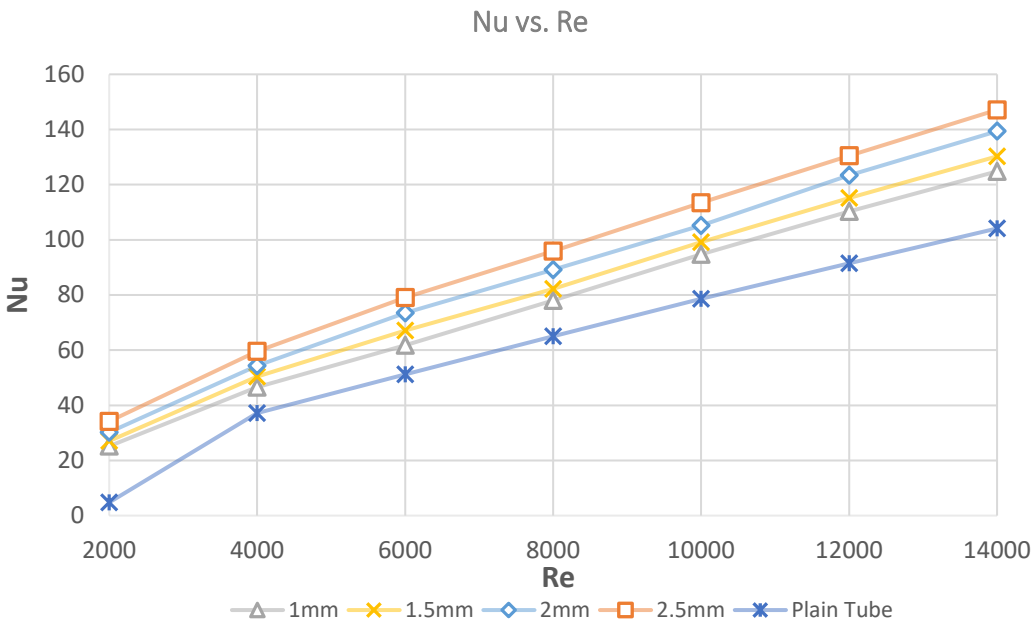

Figure 4.4 Variation of Nusselt number with Reynolds numbers at different dimple depths for water.

Figure 4.5 shows a comparison in the friction factor for different dimpled tube depths at various Reynolds numbers. The friction factor data presented in Figure 4.5 provide a better understanding of the pressure loss caused by internal walls of the tube, which in the present study, the effect of capsule dimples on pressure loss can be seen clearly. The results show that the friction factor decreases by increasing the Re and increases by increasing the dimple depth. These effects are caused by the resistance exerted by the dimples at different depths toward the flowing fluid resulting in an incremental pressure drop. As an illustration, for Re = 2,000 and dimple depth of 2.5 mm, an almost five times increase in the friction factor in relative to plain tubes can be found. On the other hand, for a dimple depth of 1 mm for the same Re, the increase in the friction factor is almost doubled. This means that at relatively low Reynolds numbers and larger dimple depths, the friction factor increases dramatically. While at higher Reynolds numbers and smaller dimple depths, it results in a reduction in the friction factor. The increase in the friction factor is mainly due to the dimples which are resisting the fluid flow.

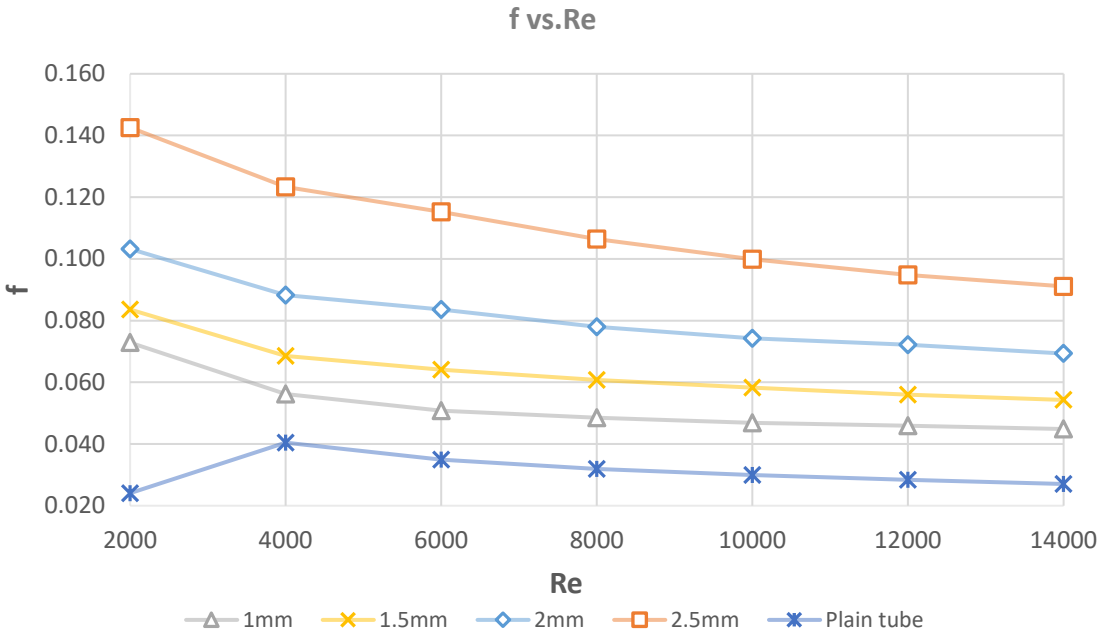

Figure 4.5 Variation of friction factor with Reynolds numbers at different dimple depths for water.

The performance evaluation criteria (PEC) is very an important tool to study the heat transfer and pressure drop within the tested tubes by implementing the capsule dimples in the tube surface and using water as a working fluid, thus evaluating the performance of that tube considering all performance effects. It is preferable to discretize the data presented in Figure 4.6 into three regions based on the interference points. Point A at Re = 4,000 representing the transition, Point B at Re = 6,000 and Point C at Re = 8,000 and above for turbulent flow. At Point A, the best dimpled tube performance according to the PEC is the one with 1.5 mm dimple depth and lowest with 2.5 mm dimple depth. At Point B, a conflict between 1 mm, 1.5 mm and 2 mm is observed; however, 2 mm is the most superior. Lastly, Point C is the breaking point for 1 mm to stay in the upper lead followed by 1.5 mm and then 2 mm. The observation of these outcomes proved to have a fluctuating pattern, thus a preference of dimple depth at each Reynolds number.

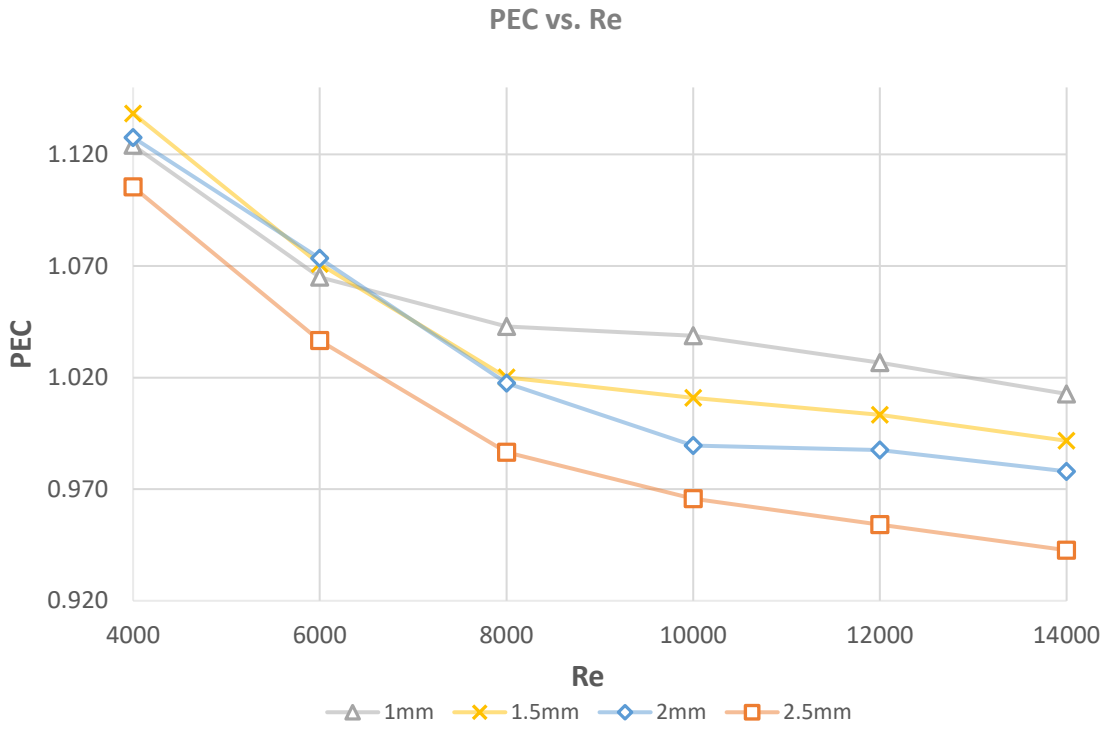

Figure 4.6 Chart of performance evaluation criteria (PEC) with Reynolds numbers at four different dimple depths.

The effect of the dimple depth for Re = 2,000 on PEC is explained in following part and is not shown on Figure 4.6 since the value of the PEC in the laminar region is very high compared to the turbulent region.

Another important finding is that even the PEC increases with dimple depth, after a specific depth, performance starts to fall because of blockages inside the pipe. For instance, when the dimple depth is very high, after 2 mm, performance starts to drop especially after Re = 6,000, and for 2.5 mm, the friction factor increases dramatically and performance drops quickly. Further discussion relating this topic can be found in Section 4.4.

4.3. THE EFFECT OF NANO FLUIDS AT DIFFERENT NANOPARTICLE CONCENTRATIONS IN THE CAPSULE DIMPLED TUBE ON HEAT TRANSFER PERFORMANCE

Three different concentrations of nanofluid (1%, 2% and 3%) were simulated to investigate the role of nanofluids along with capsule dimpled tubes on enhancing the heat transfer performance.

4.3.1. Al_2O_3-Water Nanofluid 1%

Firstly, Al_2O_3-Water nanofluid at 1% concentration is simulated for different dimple depths and different Reynolds numbers. The effects of the Nusselt number, friction factor and PEC are given in the next parts.

In Figure 4.7, a comparison on Nu between the plain tube and the capsule dimpled tube (CDT) at different dimple depths for a nanofluid as the working fluid can be seen. The figure presents the effects of the CDT at different dimple depths and various Reynolds numbers on the Nusselt number variation.

It can be seen from Figure 4.7 that increasing of the concentration of nanoparticles to 1% alongside the Reynolds number and capsule dimple depth cause the Nusselt number to increase even more compared to CDT with water and a plain tube with the same nanoparticle concentration. The increase of Nu in the laminar (Re = 2,000) region between the plain tube and CDTs are significantly high, but between the different depths of CDT, the increase is relatively low.

For the transitional region (Re = 4,000), the increase in all dimpled tubes is obvious in relation to the plain tube, as seen in Figure 4.8. Lastly, in the turbulent region, a linear pattern is observed in Nusselt number augmentation.

Among all the studied dimpled tubes at different flow velocities, the 2.5 mm dimple depth tube at Re = 14,000 shows a maximum rise in the Nu number. The opposite trend is found in 1 mm dimple depths at Re = 2,000.

For the Laminar region (Re = 2000), increasing Re along with the dimple depths causes the Nu to increase rapidly. The presence of the nanofluid as the working fluid domain showed the advantages, especially with the capsule dimples, since it strengthens the thermal conductivity of the base fluid, which in return improves the heat transfer, thereby increasing the average Nusselt number.

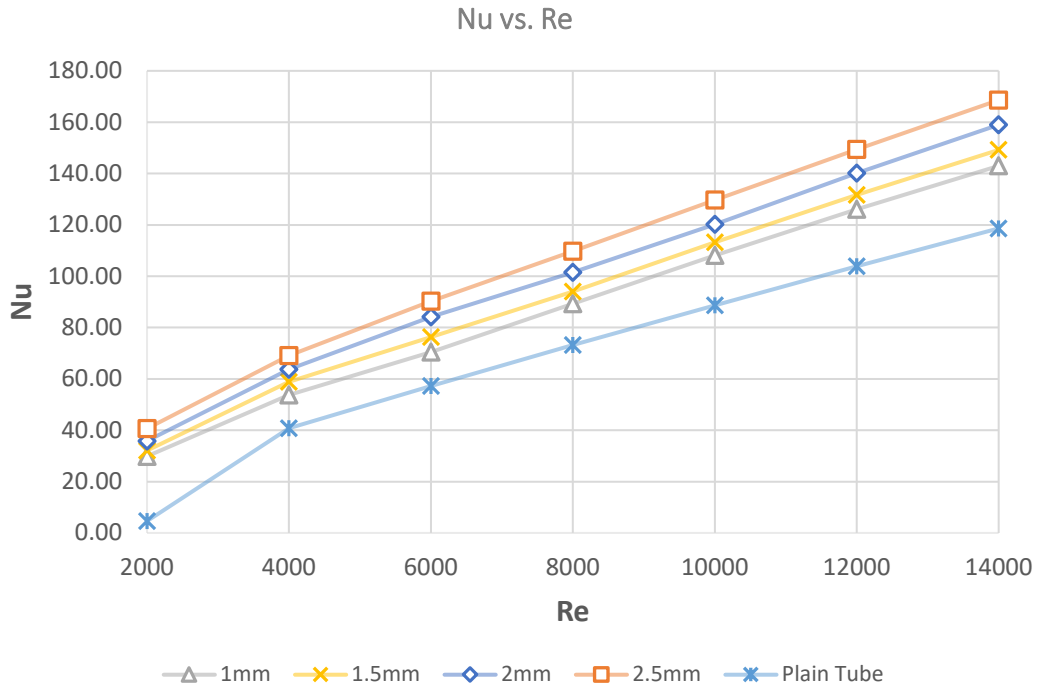

Figure 4.7 Variation of Nusselt numbers with Reynolds numbers at different dimple depths for Al_2O_3-Water nanofluid 1%.

Figure 4.8 presents a comparison of the friction factors for different dimpled tube depths at various Reynolds numbers. The friction factor data presented in Figure 4.8 provide a better understanding of the pressure loss caused by the internal walls of the tube, which in the present study is the effect of using nanofluid at 1% nanoparticle concentration in addition to capsule dimples on overall pressure loss. The results show that the friction factor decreases by increasing Re and by increasing the dimple depth. These effects are caused by the resistance exerted by the dimples at different depths toward the flowing fluid resulting in an incremental pressure drop. An important observation from Figure 4.4 is that the 1% nanoparticle concentration in the nanofluid has almost no increase in the friction factor when compared to water. In practice, due to the small size of the nanoparticles, there are no significant effect on flow behavior. Thus, increasing in friction factor will not be affected by the nanofluid compared to water (Suresh et al., 2011).

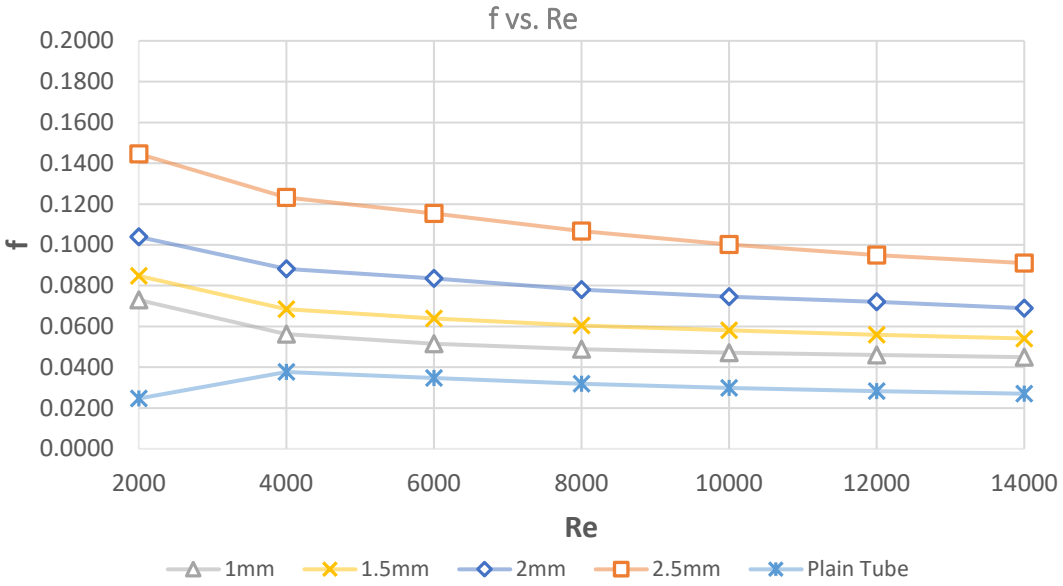

Figure 4.8 Variation of friction factor with Reynolds numbers at different dimple depths for Al_2O_3-Water nanofluid 1%.

Figure 4.9 presents the PEC for nanofluid at 1% volume concentration. Point A at Re = 4,000 is the transition, Point B at Re = 6,000 and Point C at Re = 8,000 and above are the turbulent flows. At Point A, the best dimpled tube performance according to the PEC is the one which has a 1.5 mm dimple depth and lowest with a 2.5 mm dimple depth. At Point B, a conflict between 1 mm, 1.5 mm and 2 mm is observed; however, 2 mm shows superior performance. Lastly, Point C is the breaking point for 1 mm to stay in the upper lead followed by 1.5 mm then 2 mm as expected from the increment of the Nusselt number observed in Figure 4.7 for all cases, thus affecting the PEC to increase accordingly.

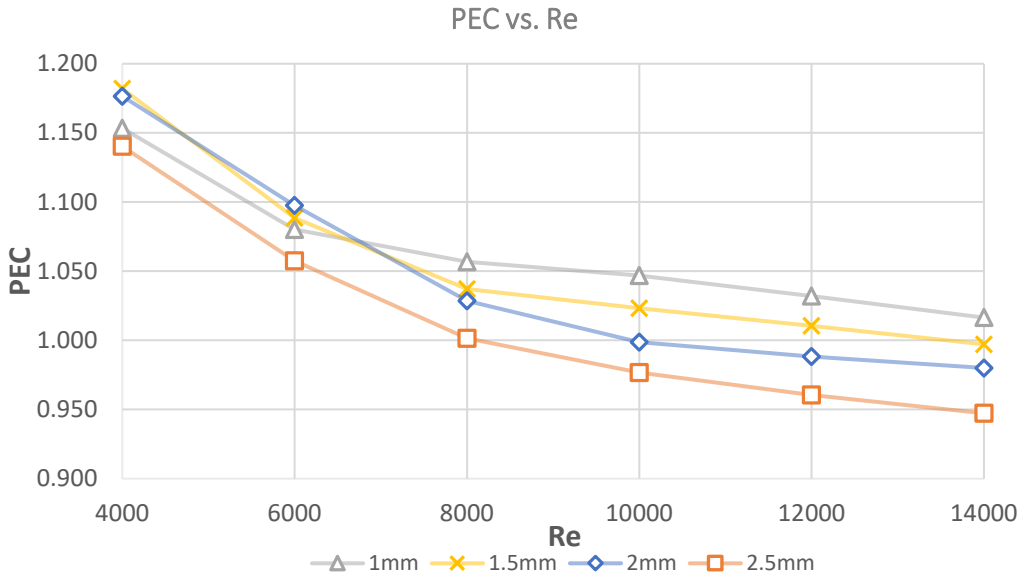

Figure 4.9 Chart of performance evaluation criteria (PEC) with Reynolds numbers in four different dimpled depths for Al_2O_3-Water nanofluid 1%.

4.3.2. Al_2O_3-Water Nanofluid 2%

Al_2O_3-Water Nanofluid at 2% concentration is simulated for different dimple depths and different Reynolds numbers. The effects of the Nusselt number, friction factor and PEC are given in the next parts.

Figure 4.10 presents a comparison of Nu between a plain tube and a capsule dimpled tube (CDT) at different dimple depths with the nanofluid as a working fluid. The figure shows the effect of the CDT at different dimple depths and different Reynolds numbers on the variation of the Nusselt number.

From Figure 4.10, it can be seen that the increase in the concentration of nanoparticles at 1% along with the Reynolds number and capsule dimple depth makes the Nusselt number increase even higher compared to the CDT with water and a plain tube with the same nanoparticle concentration. The increase of Nu in the laminar region (Re = 2000) between the plain tube and CDTs is significantly higher, but between different depths of the CDTs, the increase is relatively small.

In the transitional region (Re = 4000), the increase is significant for all dimpled tubes compared to the plain tube, as can be seen in Figure 4.7. Finally, in the turbulent region, a linear pattern is observed in the increase of the Nusselt number.

Among all the dimpled tubes studied at different flow velocities, the tube with a 2.5 mm dimple depth and a maximum increase in the Nusselt number was observed at Re = 14,000. The opposite trend is found for the 1 mm dimple depth at Re = 2,000.

For the laminar region at Reynolds number 2,000, the increase in Re along with the dimple depths leads to a rapid increase in the Nu number. Nanofluids at 2% volume concentration also showed a linear increase in the Nusselt number for all Reynolds numbers.

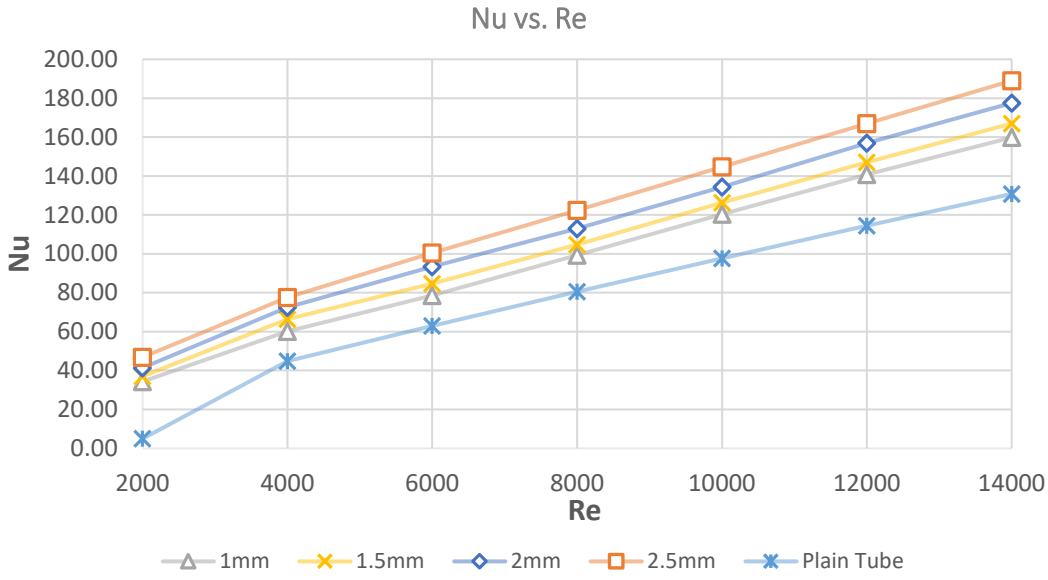

Figure 4.10 Variation of Nusselt numbers with Reynolds numbers at different dimple depths for Al_2O_3-Water nanofluid 2%.

Figure 4.11 shows a comparison of the friction factor for different dimpled tube depths at various Reynolds numbers. The friction factor results presented in Figure 4.11 provide a better understanding of the pressure drop caused by the inner tube wall. In the present study, the effect of using a nanofluid at 2% nanoparticle concentration in addition to the capsule dimples on the total pressure drop was investigated. The results showed that the friction factor would decrease when increasing Re and increase when increasing the dimple depth. These effects are caused by the resistance of the dimples at different depths exerting on the flowing fluid, resulting in an increase in the pressure drop. A similar observation is made regarding the effect of 2% nanoparticle concentrations on increasing the friction factor compared to a fluid with only water.

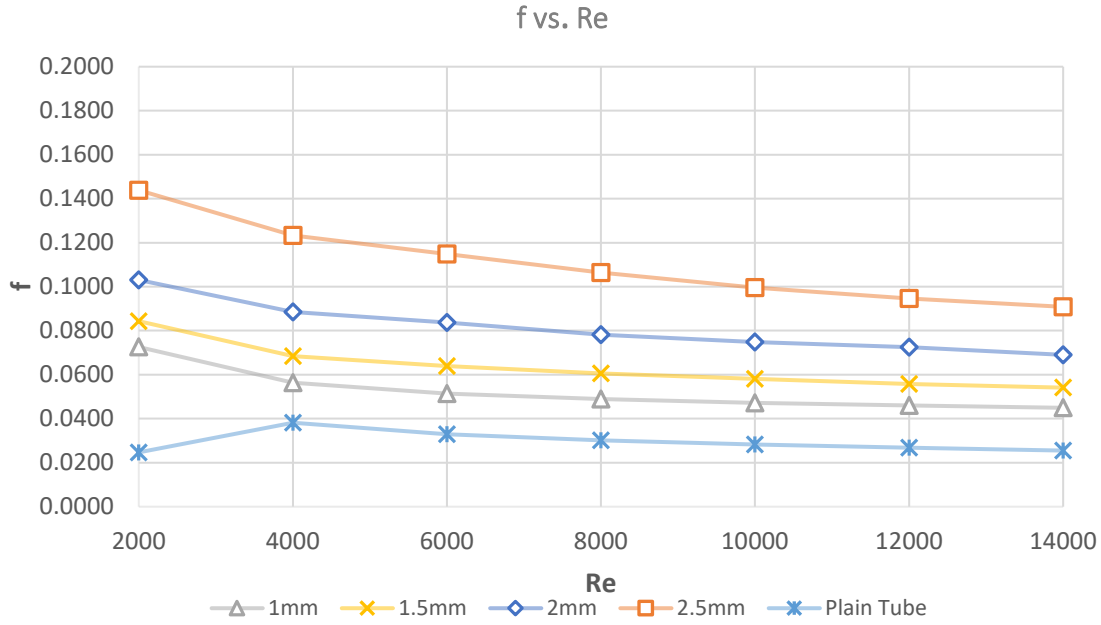

Figure 4.11 Variation of friction factor with Reynolds numbers at different dimple depths for Al_2O_3-Water nanofluid 2%.

Compared to the previous section, we proceed similarly in evaluating the performance evaluation criteria (PEC) of the capsule dimpled tube and nanofluid at 2% volume concentration as the working fluid. Figure 4.12 shows the three sections based on the interference points. Section A at Re = 4,000 shows the transition, Section B at Re = 6,000 and Section C at Re = 8,000 and above for turbulent flow. In Section A, a close relationship can be seen between depths 1.5 mm and 2 mm on the upper line and 1 mm and 2.5 mm on the lower line, where they are close to each other, respectively. In Section B, the PEC values line up close to each other, where this section can initiate the exchange between 1 mm, 1.5 mm and 2 mm. Finally, point C is the breaking point for 1 mm to remain in the top line, followed by 1.5 mm and then 2 mm. Increasing the volume concentration of the nanofluid to 2% showed an increase in the PEC accordingly.

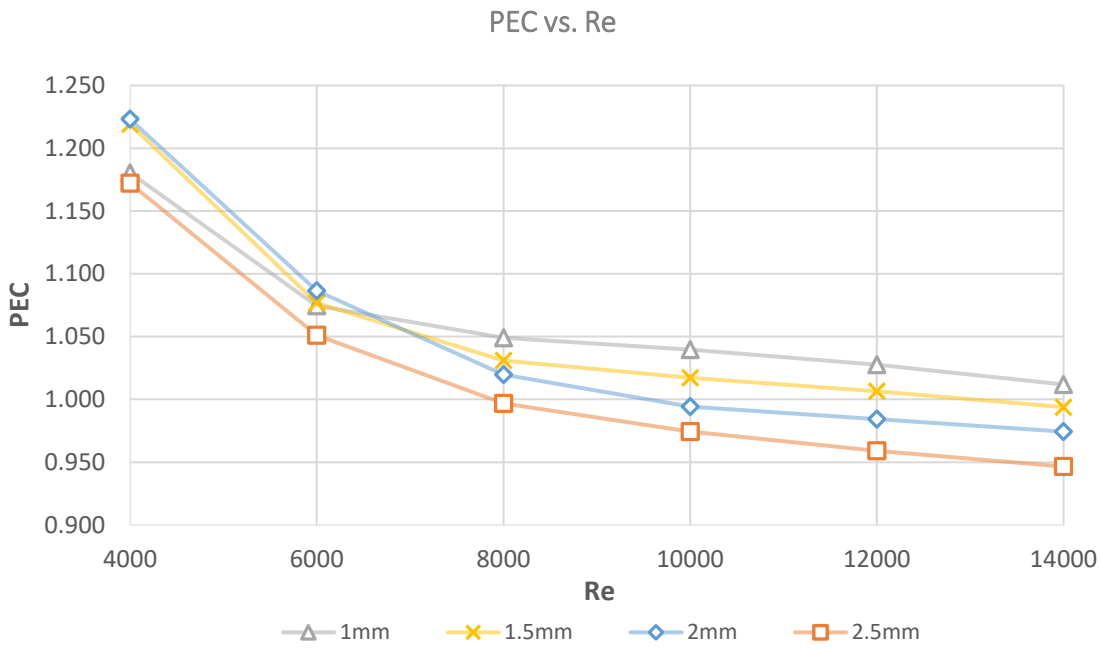

Figure 4.12 Chart of performance evaluation criteria (PEC) with Reynolds numbers in four different dimpled depths for Al_2O_3-Water nanofluid 2%.

4.3.3. Al_2O_3-Water Nanofluid 3%

When Al_2O_3-Water nanofluid at 3% nanoparticle concentration is used, the Nusselt number increases noticeably compared to both the plain tube with nanofluid for the same nanoparticle concentration (Figure 4.13) and the capsule dimple tube with a nanofluid at lower nanoparticle concentration (1% and 2%) from the previous sections. Meanwhile, when implementing the different dimple depths, the increment increases further. For instance, the ultimate increment obtained from the 2.5 mm depth is 46.34% compared to the case of using this nanofluid without a dimpled tube (plain tube). The Nusselt number also increased by increasing the Reynolds number and dimple depth.

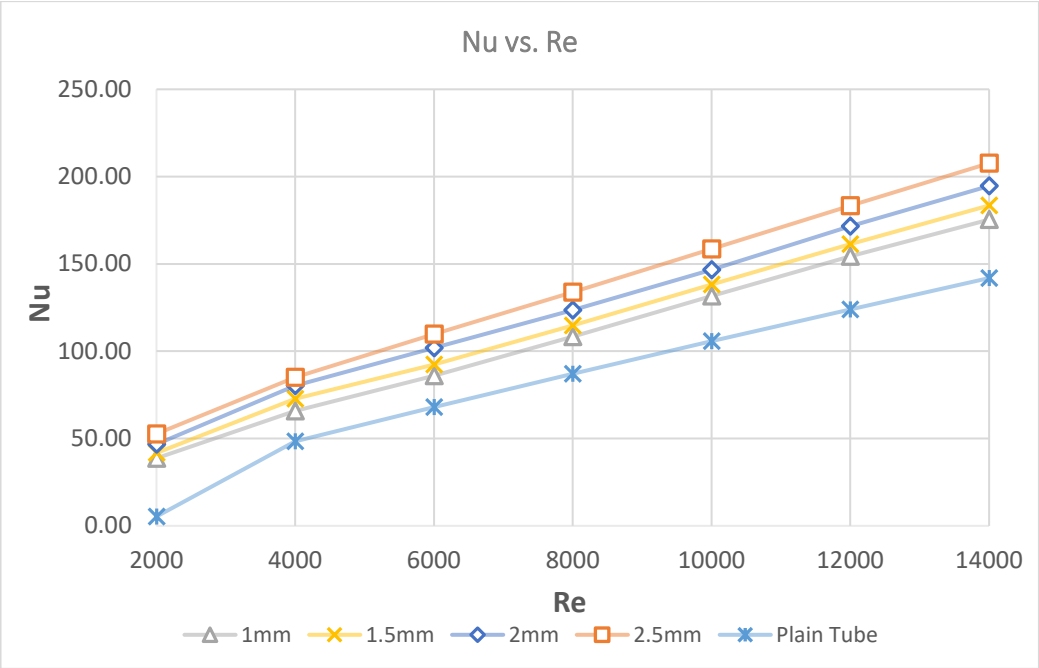

Figure 4.13 Variation of Nusselt numbers with Reynolds numbers at different dimple depths for Al_2O_3-Water nanofluid 3%.

Based on the pressure drops extracted from the simulations, the friction factor is calculated according to Equation (17). Figure 4.14 presents the influence of using a capsule dimple tube (CDT) with nanofluid at 3% nanoparticle concentration as a working fluid to the pressure drop. In comparison to the plain tube with 3% nanofluid, the cases for where the dimples at different depths are implemented, a considerable increase in friction factor occurs as an increase of the dimple depth. Upon examination, Figure 4.14 shows that the effect of the nanofluid at 3% nanoparticle concentration in a CDT on the friction factor is high compared to the plain tube. Generally, the use of nanofluids at any volume concentration in a CDT at different depths showed relatively small increases in the friction factor compared to the case with only water.

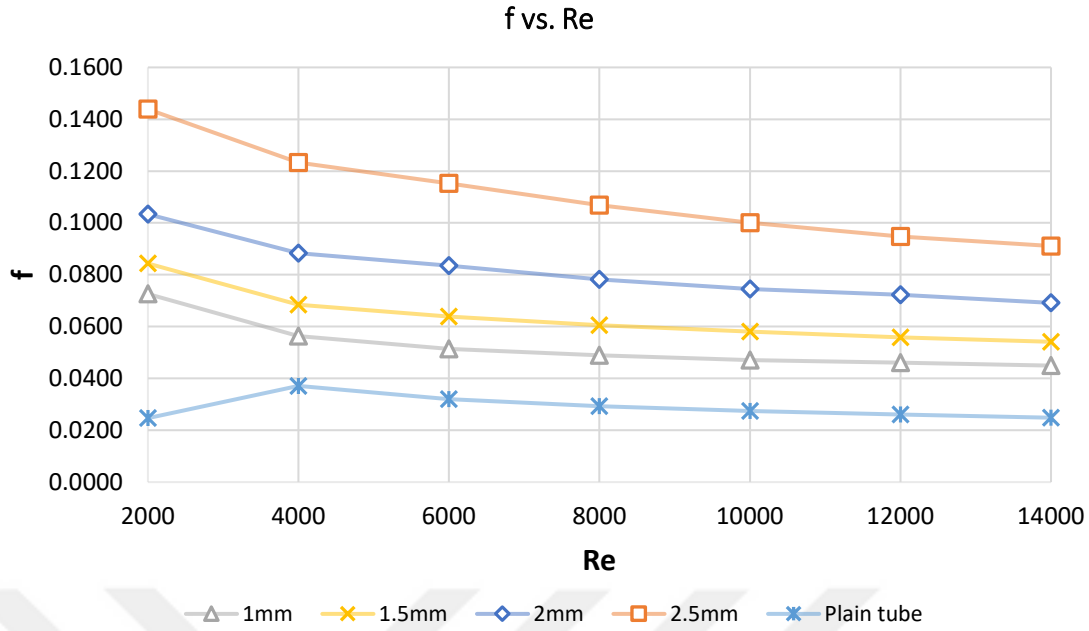

Figure 4.14 Variation of friction factor with Reynolds numbers at different dimple depths for Al_2O_3-Water nanofluid 3%.

The formulation used to calculate the PEC is given in Equation (22). Knowing that values above 1 indicate total enhancement caused by using 3% volume concentration in a nanofluid and capsule dimpled tube for different depths, it appears from Figure 4.15 that tubes with varying depths are showing variation as the Reynolds number decreases. This means that the heat transfer shows an increase. On the other hand, the friction factor decreases; however, it is still considerably high compared to the plain tube case. That is, it leads to a reduction in the PEC. Similarly, PEC distribution was also observed by Suresh et al. (2011).

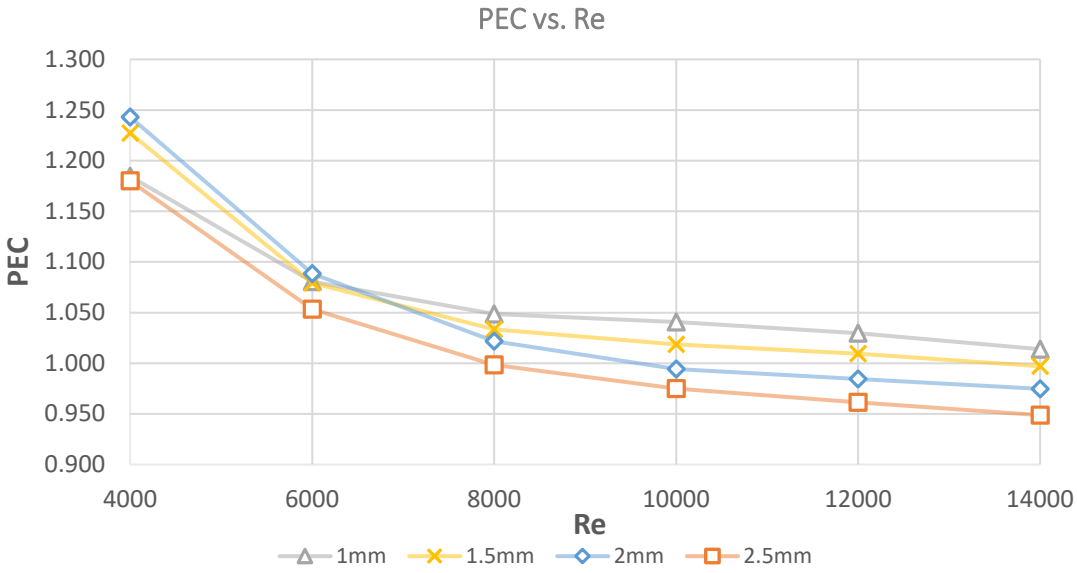

Figure 4.15 Chart of performance evaluation criteria (PEC) with Reynolds numbers in four different dimpled depths for Al_2O_3-Water nanofluid 3%.

4.4. PEC VARIATION IN CAPSULE DIMPLE DEPTHS FOR WATER AND NANOFLUID AT DIFFERENT NANOPARTICLE CONCENTRATIONS FOR DIFFERENT REYNOLDS NUMBERS

In the following discussion, the effect of dimple depths on PEC is studied at constant Reynolds numbers for laminar, transition, early turbulent and fully turbulent flows.

4.4.1. Re = 2,000 (Laminar Region)

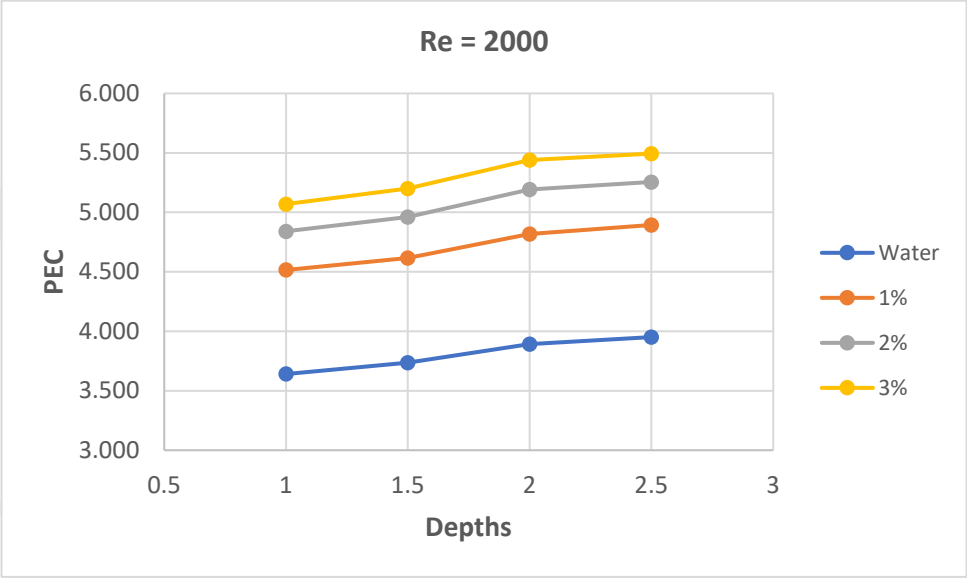

Figure 4.16 Effect of increasing dimple depth on PEC for Re = 2,000

Since the velocities are low in the laminar region, the implementation of the capsule dimple tube (CDT) at different dimple depths increases the PEC in the case of water. Consequently, using a nanofluid at different volumetric concentrations rapidly increases the PEC, which can be seen clearly in Figure 4.16. Hence, in the laminar region, the maximum PEC is noted compared to the transition and turbulent regions. Since the enhancement in the Nusselt number is overcoming the enhancement in the friction factor in this particular region, the overall performance increases.

4.4.2. Re = 4,000 (Transition)

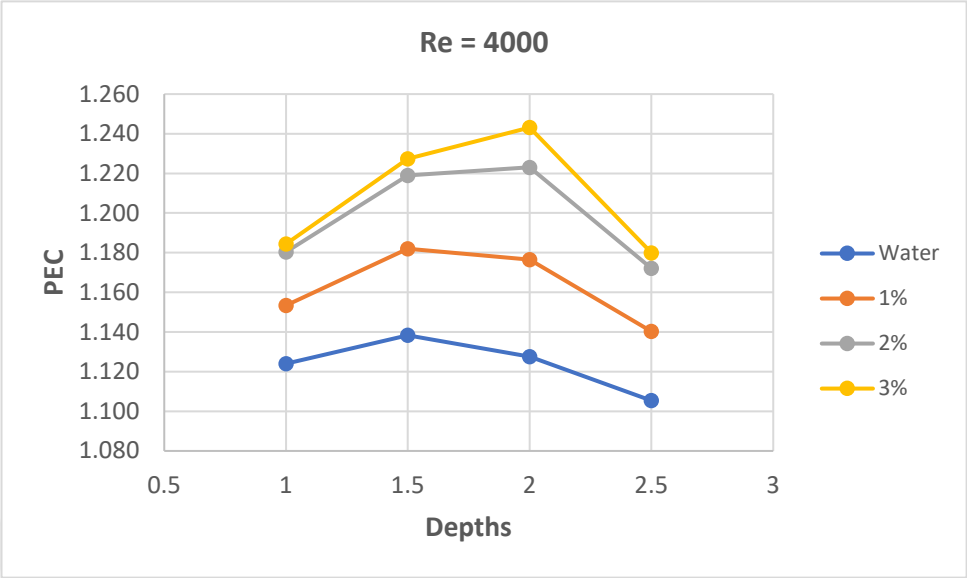

Figure 4.17 Effect of increasing dimple depth on PEC for Re = 4,000

For the transition region, an increase in volume concentration of nanofluid increases the PEC. On the other hand, as dimple depth increases, especially beyond 1.5 mm, it causes a reduction in performance mostly for only water and 1% nanofluid. It is noted that after 2 mm, there is a blockage with performance decreasing rapidly, as shown in Figure 4.17. This may be because of the unpredictable flow phenomena that relates to the transition region. Further discussion on flow blockage is found in Section 4.4.

4.4.3. Re = 6,000 (Early Turbulence)

Figure 4.18 illustrates the early formation of turbulent flow, an increasing pattern in the PEC and a sudden drop eventually. The increase in nanoparticle concentration of nanofluids shows no significant effect in this region. Nevertheless, 1% concentration showed performed best among water and other nanoparticle concentrations.

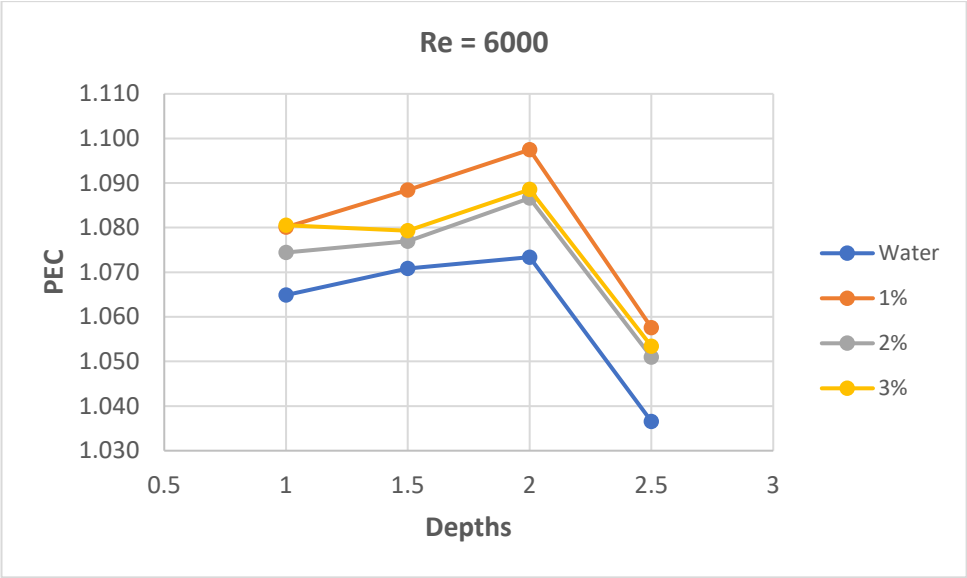

Figure 4.18 Effect of increasing dimple depth on PEC for Re = 6,000

4.4.4. Re = 10,000 (Turbulence)

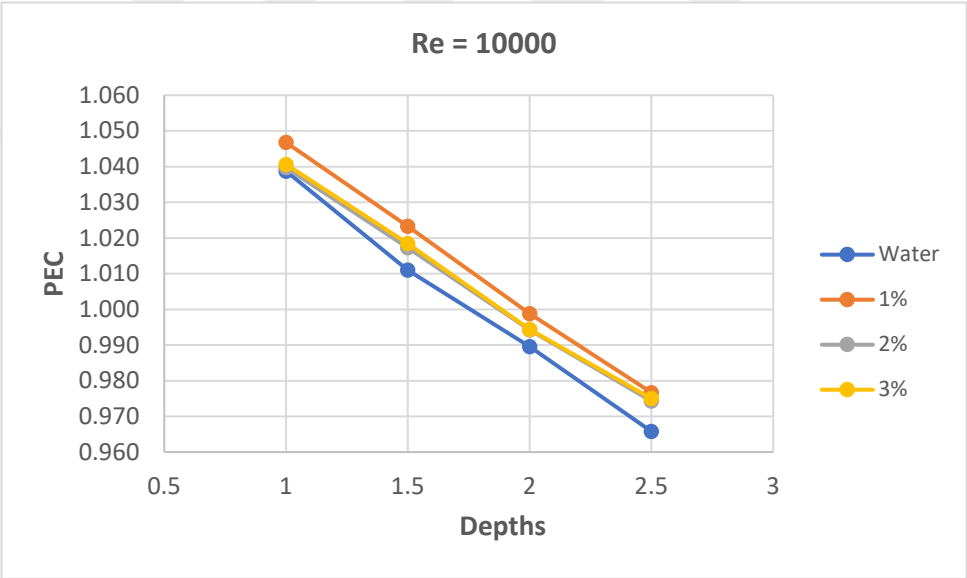

Figure 4.19 Effect of increasing dimple depth on PEC for Re = 10,000

For a high Re, Figure 4.19 shows that the dimple depth adversely affects the performance since the friction factors are very high. The PECs drop dramatically with increasing depths. Moreover, the best performance is found for 1% nanofluid and a tube with a dimple depth of 1 mm.

4.4.5. Re = 12,000 (Turbulence)

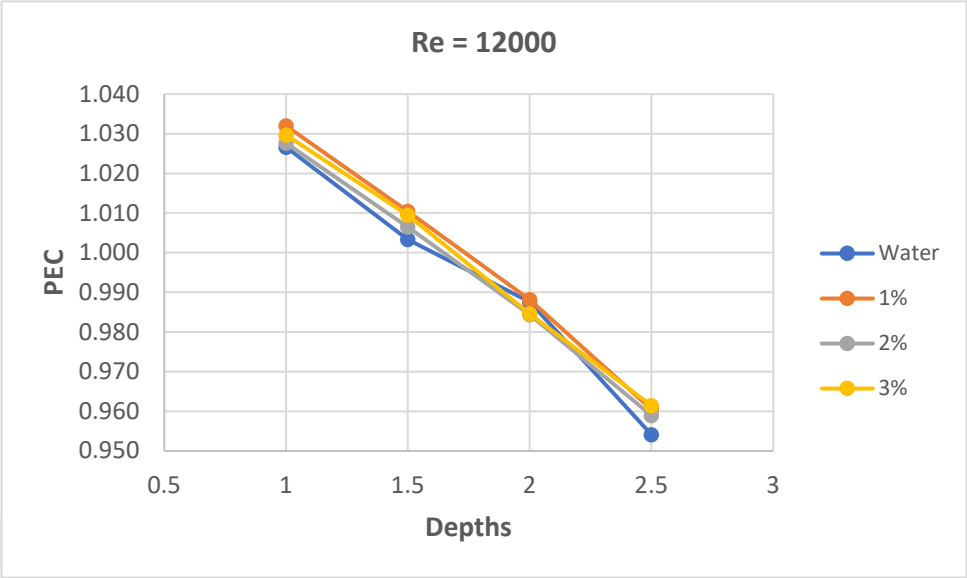

Figure 4.20 Effect of increasing dimple depth on PEC for Re = 12,000

The same trend is found for Re = 12,000, such as dimple depth adversely affecting the performance of the capsule dimple tube due to the high resistance acted against the flow. The best performance is also found for 1% nanofluid with a dimple depth of 1 mm, as seen in Figure 4.20.

4.5 EFFECTS OF BLOCKAGE ON PERFORMANCE EVALUATION CRITERIA (PEC) BY CONSIDERING THE REDUCTION IN FLOW AREA.

To see the effect of area blockage, a study is conducted for another tube diameter and calculating the area ratio where the blockage starts. Moreover, two tube diameters (14 mm and 18 mm) are compared to each other by considering PEC drops at constant Reynolds numbers and different dimple depths.

4.5.1 PEC at Different Depths for the Transition and Turbulent region.

Figures 4.21 and 4.22 show the PEC drop due to blockage caused by increasing the dimple depth. For a better understanding, the area ratio is calculated by dividing the circular tube cross sectional area over the dimpled tube cross sectional area at different dimple depths. Thus, an observation is formed by comparing the depth in which the PEC drop is taking place at each diameter (14 mm and 18 mm) and comparing it to the area ratios, as shown in Table 4.1, to conclude that it is likely for the blockage to initiate after a ratio of 0.91 to 0.95, which indicates a 1.5 mm depth for both diameters.

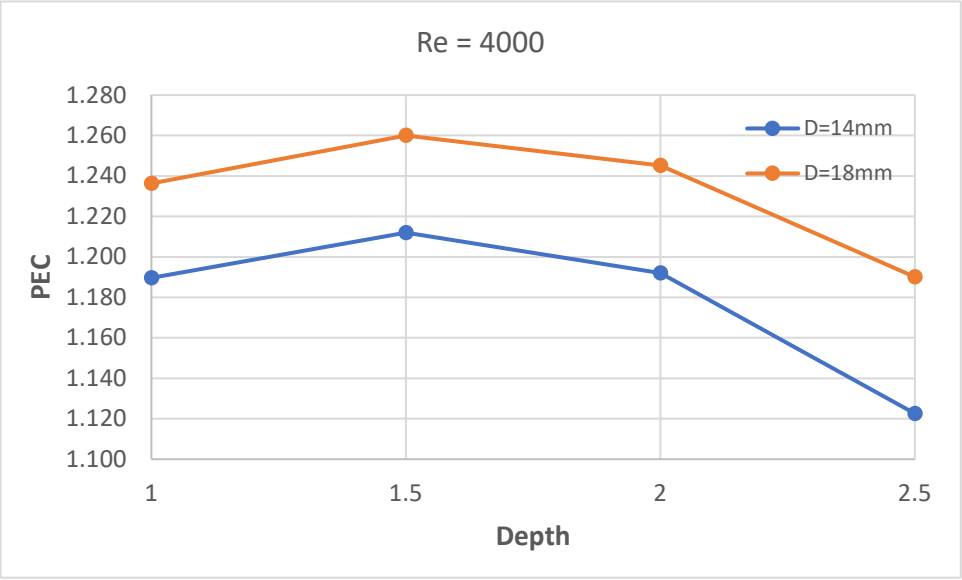

Figure 4.21 PEC drop at different tube diameters for Re = 4,000

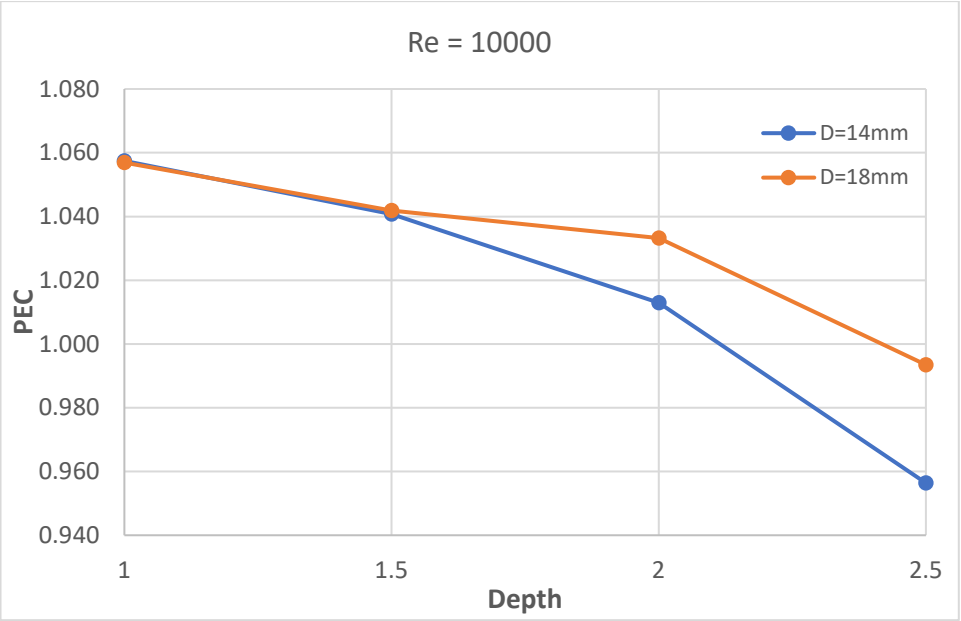

Figure 4.22 PEC drop at different tube diameters for Re = 10,000

The area ratio is calculated by dividing the circular tube cross sectional area (A_t) over the dimpled tube cross sectional area at different dimple depths (A_d). Table 4.1 presents the area ratio of tubes with 14 mm and 18 mm diameters at different dimple depths.

$$\text{Area ratio} = \frac{A_d}{A_t} \tag{34}$$

Table 4.1 Tube cross sectional area ratio at different depths.

Diameter	14 mm	18 mm
Depth	1 mm	1 mm
Area Ratio	0.96	0.98
Depth	1.5 mm	1.5 mm
Area Ratio	0.91	0.95
Depth	2 mm	2 mm
Area Ratio	0.85	0.91
Depth	2.5 mm	2.5 mm
Area Ratio	0.76	0.85

CHAPTER 5

CONCLUSION

5.1 CONCLUSIONS

A numerical investigation was carried out on convective heat transfer, pressure drop characteristics and performance evaluation criteria (PEC) for newly proposed capsule dimple tubes with and without an Al_2O_3-Water based nanofluid as the heat transfer fluid under fully developed laminar, transition and turbulence flow conditions with uniform heat flux. The simulations were performed using the computational fluid dynamic (CFD) commercial software Fluent ANSYS 20R1. 3-D Capsule dimple tube and 2-D Plain tubes were simulated assuming a steady state flow with uniform velocity at the inlet under constant heat flux. Two main parameters were the focus throughout this study which had a direct impact on the Nusselt number, friction factor and PEC, at different dimple depths varying between 1 mm and 2.5 mm and different concentrations of Al_2O_3-Water nanofluid (1%, 2% and 3%). The Reynolds numbers for the analyzed cases in this study ranged from 2,000 to 14,000.

The findings through this investigation can be divided into two main sections based on the heat transfer fluid used, which in our case was water and Al_2O_3-Water nanofluid. Under each section, different dimple depths were studied. Additionally, under the nanofluid section, three different nanoparticle concentrations were studied for each dimple depth.

According to the results obtained in Section 1 (water as the heat transfer fluid), increasing dimple depth had a significant influence on increasing the Nusselt number as the Reynolds number increased. In contrast, the friction factor would increase accordingly as dimple depth increased and the Reynolds number would decrease compared to a plain tube. As a result, the PEC showed a more significant increase in the laminar region than in the transition and gradually it would decrease in the turbulent region (Figures 4.6 and 4.16).

In Section 2 (Al_2O_3-Water as the heat transfer fluid), the results were similar to those of Section 1, where the Nusselt number, friction factor and PEC would increase. Furthermore, as nanoparticle concentration increases for each dimple depth, the Nusselt number increases and the friction factor increases obviously compared to plain tube (Al_2O_3-Water).

Another finding is the blockage phenomena, observed when dimple depths become deeper. This acts as barrier against fluid flow, which in turn results in an increase in the friction factor and a decrease in PEC.

In summary, when considering PEC, the best performance among all the studied cases based on flow field are found as follows:

- Laminar region (Re = 2,000), 2.5 mm dimple depth and 3% nanoparticle concentration.
- Transition region (Re = 4,000), 2 mm dimple depth and 3% nanoparticle concentration.
- Early turbulence region (Re = 6,000), 2 mm dimple depth and 1% nanoparticle concentration.
- Turbulence region (Re ≥ 8,000), 1 mm dimple depth and 1% nanoparticle concentration.

Regarding the findings, for small Re (laminar flow), higher depths seem to have a better performance probably due to the huge increase in Nusselt number for dimple tube compared to plain tube.

For transition flow a specific depth is shown to have a better performance as volume concentration increases.

In the other hand, high Re in the turbulent region, proved that increasing nanoparticle concentration has less effect on increasing PEC, since deeper dimples causes the friction factor to increase very much.

The combination of capsule dimples and Al_2O_3-Water based nanofluid used in this study considered as a novelty which have not been studied deeply by other researchers.

5.2 FUTURE WORKS

The following are recommendations for future studies:

- A numerical investigation using a multi-phase nanofluid model (instead of a single phase model) and comparing it with current studies.
- Applying hybrid nanofluids, such as Al_2O_3 and TiO_2 nanoparticles in a water based fluid.
- Analyzing the effects of changing capsule dimple orientations on performance evaluation criteria (PEC).
- Conducting an experimental study on capsule dimpled tubes under the same boundary conditions and comparing them with the current study.

REFERENCES

Alshehri, F., Goraniya, J., & Combrinck, M. L. (2020). Numerical investigation of heat transfer enhancement of a water/ethylene glycol mixture with Al_2O_3–TiO_2 nanoparticles. Applied Mathematics and Computation, 369, 124836.

Batchelor, G. K. (1977). The effect of Brownian motion on the bulk stress in a suspension of spherical particles. Journal of fluid mechanics, 83(1), 97-117.

Briclot, A., Henry, J. F., Popa, C., Nguyen, C. T., & Fohanno, S. (2020). Experimental investigation of the heat and fluid flow of an Al_2O_3-water nanofluid in the laminar-turbulent transition region. International Journal of Thermal Sciences, 158, 106546.

Cengel, Y. (2014). Heat and mass transfer: fundamentals and applications. McGraw-Hill Higher Education.

Chandrasekar, M., Suresh, S., & Bose, A. C. (2010). Experimental studies on heat transfer and friction factor characteristics of Al2O3/water nanofluid in a circular pipe under laminar flow with wire coil inserts. Experimental Thermal and Fluid Science, 34(2), 122-130.

Chen, J., Müller-Steinhagen, H., & Duffy, G. G. (2001). Heat transfer enhancement in dimpled tubes. Applied thermal engineering, 21(5), 535-547.

Cheraghi, M. H., Ameri, M., & Shahabadi, M. (2020). Numerical study on the heat transfer enhancement and pressure drop inside deep dimpled tubes. International Journal of Heat and Mass Transfer, 147, 118845.

Eiamsa-Ard, S., & Promvonge, P. (2007). Heat transfer characteristics in a tube fitted with helical screw-tape with/without core-rod inserts. International Communications in Heat and Mass Transfer, 34(2), 176-185.

Firoozi, A., Majidi, S., & Ameri, M. (2020). A numerical assessment on heat transfer and flow characteristics of nanofluid in tubes enhanced with a variety of dimple configurations. Thermal Science and Engineering Progress, 19, 100578.

Gee, D. L., & Webb, R. L. (1980). Forced convection heat transfer in helically rib-roughened tubes. International Journal of Heat and Mass Transfer, 23(8), 1127-1136.

Göktepe, S., Atalık, K., & Ertürk, H. (2014). Comparison of single and two-phase models for nanofluid convection at the entrance of a uniformly heated tube. International Journal of Thermal Sciences, 80, 83-92.

Ho, C. J., Chang, C. Y., Yan, W. M., & Amani, P. (2018). A combined numerical and experimental study on the forced convection of Al_2O_3-water nanofluid in a circular tube. International Journal of Heat and Mass Transfer, 120, 66-75.

Khedkar, R. S., Sonawane, S. S., & Wasewar, K. L. (2014). Heat transfer study on concentric tube heat exchanger using TiO2–water based nanofluid. International communications in Heat and Mass transfer, 57, 163-169.

Kukulka, D. J., & Smith, R. (2013). Thermal-hydraulic performance of Vipertex 1EHT enhanced heat transfer tubes. Applied Thermal Engineering, 61(1), 60-66.

Kumar, A., Maithani, R., & Suri, A. R. S. (2017). Numerical and experimental investigation of enhancement of heat transfer in dimpled rib heat exchanger tube. Heat and Mass Transfer, 53(12), 3501-3516.

Liu, B. Y., & Agarwal, J. K. (1974). Experimental observation of aerosol deposition in turbulent flow. Journal of Aerosol Science, 5(2), 145-155.

Manual, U. D. F. (2009). ANSYS FLUENT 12.0. Theory Guide. Canonsburg, PA.

Maxwell, J. C. (1954). Electricity and magnetism (Vol. 2). New York: Dover.Corcione, M. (2011). Empirical correlating equations for predicting the effective thermal conductivity and dynamic viscosity of nanofluids. Energy Conversion and Management, 52(1), 789-793.

Mehrjou, B., Heris, S. Z., & Mohamadifard, K. (2015). Experimental study of CuO/water nanofluid turbulent convective heat transfer in square cross-section duct. Experimental Heat Transfer, 28(3), 282-297.

Menlik, T., Sözen, A., Gürü, M., & Öztaş, S. (2015). Heat transfer enhancement using MgO/water nanofluid in heat pipe. Journal of the Energy Institute, 88(3), 247-257.

Minea, A. A. (2017). Hybrid nanofluids based on Al_2O_3, TiO_2 and SiO_2: numerical evaluation of different approaches. International Journal of Heat and Mass Transfer, 104, 852-860.

Mohapatra, K., & Mishra, D. P. (2015). Effect of fin and tube configuration on heat transfer of an internally finned tube. International journal of numerical methods for heat & fluid flow.

Pak, B. C., & Cho, Y. I. (1998). Hydrodynamic and heat transfer study of dispersed fluids with submicron metallic oxide particles. Experimental Heat Transfer an International Journal, 11(2), 151-170.

Pak, B. C., & Cho, Y. I. (1998). Hydrodynamic and heat transfer study of dispersed fluids with submicron metallic oxide particles. Experimental Heat Transfer an International Journal, 11(2), 151-170.

Pathipakka, G., & Sivashanmugam, P. (2010). Heat transfer behavior of nanofluids in a uniformly heated circular tube fitted with helical inserts in laminar flow. Superlattices and Microstructures, 47(2), 349-360.

Peyghambarzadeh, S. M., Hashemabadi, S. H., Hoseini, S. M., & Jamnani, M. S. (2011). Experimental study of heat transfer enhancement using water/ethylene glycol based nanofluids as a new coolant for car radiators. International communications in heat and mass transfer, 38(9), 1283-1290.

Sabir, R., Khan, M. M., Sheikh, N. A., Ahad, I. U., & Brabazon, D. (2020). Assessment of thermo-hydraulic performance of inward dimpled tubes with variation in angular orientations. Applied Thermal Engineering, 170, 115040.

Siricharoenpanich, A., Wiriyasart, S., & Naphon, P. (2021). Study on the thermal dissipation performance of GPU cooling system with nanofluid as coolant. Case Studies in Thermal Engineering, 25, 100904.

Suresh, S., Chandrasekar, M., & Sekhar, S. C. (2011). Experimental studies on heat transfer and friction factor characteristics of CuO/water nanofluid under turbulent flow in a helically dimpled tube. Experimental Thermal and Fluid Science, 35(3), 542-549.

Tabatabaeikia, S., Mohammed, H. A., Nik-Ghazali, N., & Shahizare, B. (2014). Heat transfer enhancement by using different types of inserts. Advances in Mechanical Engineering, 6, 250354.

Vicente, P. G., García, A., & Viedma, A. (2002). Heat transfer and pressure drop for low Reynolds turbulent flow in helically dimpled tubes. International journal of heat and mass transfer, 45(3), 543-553.

Wang, Y., He, Y. L., Lei, Y. G., & Zhang, J. (2010). Heat transfer and hydrodynamics analysis of a novel dimpled tube. Experimental thermal and fluid science, 34(8), 1273-1281.

RESUME

PERSONAL INFORMATION

Name, Surname: Mahmoud Awni A. Haj ibrahim.

EDUCATION

Degree	Graduated school	Graduation year
High school	Ibin Baz High School	2014
Bachelor	Türk Hava Kurumu university	2018
Master	Çankaya university	2021

LANGUAGE SKILLS

Arabic – Mother tongue

English – professional

Turkish – intermediate